Dynamical analysis of the oceanic circulation in the Gulf of San Jorge, Argentina

Elbio D. Palma, Ricardo P. Matano, Mariano H. Tonini, Patricia Martos, Vincent Combes

PII: S0924-7963(19)30398-7

DOI: https://doi.org/10.1016/j.jmarsys.2019.103261

Reference: MARSYS 103261

To appear in: *Journal of Marine Systems*

Received date: 8 March 2019

Revised date: 14 September 2019

Accepted date: 6 November 2019

Please cite this article as: E.D. Palma, R.P. Matano, M.H. Tonini, et al., Dynamical analysis of the oceanic circulation in the Gulf of San Jorge, Argentina, *Journal of Marine Systems*(2019), https://doi.org/10.1016/j.jmarsys.2019.103261

Title:

Dynamical Analysis of the Oceanic Circulation in the Gulf of San Jorge, Argentina

Authors:

Elbio D. Palma[1*], Ricardo P. Matano[2], Mariano H. Tonini[3], Patricia Martos[4] and Vincent Combes[2]

Affiliations:

[1]Departamento de Física, Universidad Nacional del Sur e Instituto Argentino de Oceanografía (CONICET), Bahía Blanca, Argentina.

[2]College of Earth, Ocean and Atmos. Sc., Oregon State University, Corvallis, OR, USA.

[3]Centro para el Estudio de Sistemas Marinos (CENPAT-CONICET), Puerto Madryn, Argentina.

[4]Departamento de Ciencias Marinas, Universidad Nacional de Mar del Plata e Instituto Nacional de Investigación y Desarrollo Pesquero (INIDEP), Mar del Plata, Argentina.

***Corresponding Author:**

Dr. Elbio D. Palma
Professor
Departamento de Física
Universidad Nacional del Sur
Senior Researcher
Instituto Argentino de Oceanografía (CONICET)
(8000) Bahía Blanca, Argentina
Contact: +54-291-4558109 2814 (office)
Email: uspalma@criba.edu.ar

Keywords:

Gulf of San Jorge; Patagonian Shelf; Numerical circulation model; Seasonal Variability; Tidal and wind forcing; Cross-shelf exchanges.

Dynamical Analysis of the Oceanic Circulation in the Gulf of San Jorge, Argentina

Elbio D. Palma[1*], Ricardo P. Matano[2], Mariano H. Tonini[3], Patricia Martos[4] and Vincent Combes[2]

[1]Departamento de Física, Universidad Nacional del Sur e Instituto Argentino de Oceanografía (CONICET), Bahía Blanca, Argentina.

[2]College of Earth, Ocean and Atmos. Sc., Oregon State University, Corvallis, OR, USA

[3]Centro para el Estudio de Sistemas Marinos (CENPAT-CONICET), Puerto Madryn, Argentina.

[4]Departamento de Ciencias Marinas, Universidad Nacional de Mar del Plata e Instituto Nacional de Investigación y Desarrollo Pesquero (INIDEP), Mar del Plata, Argentina.

Abstract

This study identifies the dynamical mechanisms driving seasonal variations in oceanic circulation and water mass characteristics of the Gulf of San Jorge (GSJ) and its exchanges with the Patagonian Shelf (PS). A suite of process-oriented numerical experiments indicates that GSJ circulation is mainly driven by tidal forcing and modulated by wind forcing and intrusions from the PS. During late spring and summer, stratification decouples the upper and deeper layers of the gulf, leading to a shallow, wind-forced surface circulation and a deeper, density driven, cyclonic geostrophic flow. The subsurface circulation is induced by differential tidal mixing in coastal and deep areas and its intensity is strongly affected by the temporal variability of the atmospheric heat flux, which increases from spring to summer and fades from fall to winter. As stratification weakens, circulation patterns are replaced by wind-driven anticyclonic gyres in the south and an open cyclonic loop in the north. Passive tracer diagnostics show that in summer, surface and subsurface waters from the GSJ northern coast are exported and replaced by waters from the coastal portion of PS currents. The renewal of bottom waters is slower: A small portion upwells in the southwestern coast but most are ventilated by winter convection in the southern region and by intrusions of PS waters in the northern region.

1. Introduction

The Gulf of San Jorge (GSJ) is the largest coastal embayment of the Patagonian Shelf (PS), one of the most productive portions of the South Atlantic Ocean (Marrari et al., 2017, Fig. 1a). The GSJ's economically important fishing (Temperoni et al., 2018; Glembocki et al., 2015; Bogazzi et al., 2005) and oil industries (Silwan, 2007) face complex management problems due to the lack of information about the oceanographic characteristics of the region. Fisheries management, for example, imposes spatial and temporal restrictions on fishing activities in certain areas but the links between stock dynamics and ocean circulation are poorly understood (Glembocki et al., 2015). Likewise, oil related activities—including production, offshore drilling and transit of tankers—generate environmental risks that cannot be assessed without proper information about oceanic circulation. Furthermore, regional oil and fishing industries encompass important reproductive and foraging grounds of many marine birds and mammals (Torres et al., 2016). Therefore, a quantitative knowledge and dynamical understanding of the three-dimensional GSJ circulation is not only of physical, but also of biological and environmental importance for this region.

The limit between the GSJ and the adjacent Patagonian Shelf (PS) extends 250km from Cape Tres Puntas (47°S) to Cape Dos Bahías (45°S), encompassing a depth range of 40 to 90m (Fig. 1b). The GSJ basin is shallow and wide with a gentle 100m depression that will be referred as the Central Basin (CB) (Fig. 1b). The Subantarctic Shelf Waters and low salinity waters from the Magellan Strait intruding into the GSJ are advected northward by the Patagonian Current (Palma and Matano, 2012, Matano and Palma, 2018). There are no river discharges along the GSJ's perimeter. The annual mean wind stress distribution is characterized by a band of strong westerlies that intensifies during late fall and winter (Palma et al. 2004a, Combes and Matano, 2014a, Matano and Palma, 2018). The tidal cycle over the adjacent shelf is dominated by the M_2 semidiurnal component, which propagates northeastward. Tidal amplitudes are higher than 4m near Pta. Loyola (~51°S) and

decrease to 2m at Comodoro Rivadavia on the western coast of GSJ. The interaction of tidal currents with the shallow banks located near Cape Tres Puntas generates the third largest tidal dissipation center of the PS (Palma et al., 2004b).

There are few studies of GSJ circulation. Hydrographic surveys report the presence of waters drawn from the Magellan Strait at intermediate depths and an intense thermohaline front at the southern end of the GSJ during fall (Krock et al., 2015). Glembocki et al. (2015) identified thermal fronts along the southern and northern coasts and a major frontal area close to the mouth which extends offshore. Early modeling studies described the barotropic circulation generated by tidal and wind forcing. Tonini et al. (2006) identified a tidal dissipation center over the South Bank (SB, Fig. 1b) and a circulation regime of opposing gyres in the northern and southern portions of the gulf with accompanying coastal wind-driven upwelling/downwelling centers. More recently, Matano and Palma (2018) used a regional model to characterize the time mean circulation of the GSJ and its seasonal variations. Here we expand that study by including the results of a suite of process-oriented simulations to further identify the dynamical mechanisms underlying GSJ circulation and its interactions with the PS, including an assessment of water mass sources and residence times.

2. Model description

The numerical model used in this study is based on ROMS-Agrif (Debreu et al., 2012). In the vertical, the model's primitive equations are discretized over variable topography using stretched terrain-following coordinates. The stretched coordinates allow increased resolution in areas of interest, such as surface and bottom boundary layers. In the horizontal, the primitive equations are evaluated using orthogonal curvilinear coordinates on a staggered Arakawa C-grid. The model domain extends from 58º to 38º S and from 69º to 54º W with 1/24˚ degree horizontal resolution (Fig. 1a). It covers the entire PS and adjacent deep ocean to properly resolve GSJ-shelf interactions. In the vertical the model equations are discretized into 40 sigma levels, with higher vertical

resolution at the top and bottom layers. The bathymetry is based on digitized nautical charts (Fig. 1b).

The model has four open boundaries where radiation and advection conditions are imposed (Marchesiello et al., 2001). In our most realistic experiment (BENCH) the model is forced at these lateral boundaries with the amplitudes and phases of the M_2 tide interpolated from a global TP0X6 tidal model (Egbert et al., 1994) and the climatological temperature, salinity and velocity fields extracted from a regional model of the entire Southwestern Atlantic region at 1/12° horizontal resolution (CM14; Combes and Matano, 2014a). Further analysis of the CM14 model, including comparison with in-situ and satellite observations, is presented in Combes and Matano (2014a, 2014b, 2018), Matano et al. (2014) and Strub et al. (2015).

At the surface the model is forced with the mean climatological wind stress derived from 1999-2012 Quikscat-ASCAT climatology, and heat and freshwater fluxes derived from the Comprehensive Ocean-Atmosphere Data Set (COADS) (Da Silva et al., 1994). The heat flux equation includes a tendency restoring term to the CM14 SST climatology (Barnier, 1998). Vertical mixing is parameterized with a K-Profile Parameterization (KPP) scheme (Large et al., 1994) and bottom friction with a quadratic formulation. There is no explicit horizontal mixing included in the model simulations.

The BENCH experiment is initialized with the January climatology of the World Ocean Atlas (WOA, Conkright et al., 2002) and subsequently integrated for five years with a time step of 270 s. Model analysis is based on the results of the last year of the numerical integration. A suite of sensitivity experiments identifies the contribution of environmental variables and forcing mechanisms (e.g., PS inflows, local winds and tides) to the GSJ circulation (Table I).

3. Benchmark experiment

The depth-averaged seasonal circulation produced by BENCH is described in Matano and Palma (2018). For the sake of completeness we include a brief description here.

The seasonal circulation in GSJ is characterized by two distinct modes, corresponding to the summer (JFM) and winter (JAS) seasons, connected by transition structures during fall (AMJ) and spring (OND). The summer mode is dominated by a gulf-wide cyclonic pattern and strong interaction with the PS (Fig. 1c). During this season the inner portion of the Patagonian Current intrudes into the GSJ generating the Southern Loop Current, (SLC), which merges with an intense cyclonic coastal current (CCC). The CCC is stronger in the southern sector with partial eastward leaking into the interior near 46ºS. SLC and CCC enclose a recirculating cyclonic gyre over the CB (the Southern Cyclonic Gyre, SCG). In the northern sector the CCC is interrupted near the coast by a weak and elongated anticyclonic coastal gyre while the interior circulation is composed of a sluggish anticyclonic gyre bounded in the west by the CCC and by a broad northward flowing current in the east. These two currents reunite before exiting the GSJ through its northern edge (Cape Dos Bahías) as an intense jet.

From late fall to early winter the Patagonian Current moves offshore, thus reducing its penetration into the gulf. During winter, weakening of the density stratification dampens the cyclonic circulation, which is replaced by anticyclonic patterns in the southern region. Increasing stratification during spring leads to an intensification and expansion of the cyclonic circulation and, by the end of December, the summer circulation pattern is fully developed. Superimposed on these seasonal circulation patterns is an anticyclonic gyre over the SB (the Southeastern Anticyclonic Gyre, SEAG, Fig. 1c) that persists year-round.

The following sections describe BENCH results not discussed in Matano and Palma (2018), including analysis of the three dimensional structure of the water mass composition and circulation fields, quantification of the exchanges with the PS, identification of water sources and analysis of retention times.

3.1. Circulation and water masses

The circulation's three-dimensional structure is portrayed by the density and velocity fields vertically averaged in three layers (Fig. 2). The particular choice of sigma layers was guided by the summer flow structure (Suppl. Fig. A) to exemplify the different dynamical balances of the region. The upper and bottom layers are frictional regions largely controlled by wind forcing and tides. Circulation in the intermediate layer is more geostrophically balanced, which in addition to the influence exerted by the upper and lower layers reflects intense exchanges with the PS. During summer the Patagonian Current, which carries cold and fresh waters partly drawn from the Magellan Strait, splits into several subsurface jets that intrude into the GSJ (Fig. 2b, Fig. 3b and Suppl. Fig. A, panel b). Once entrained, these waters are warmed by solar heating and mixing, particularly in the northern region. The CCC and the SEAG are mainly composed of low density waters from surface to bottom while the SCG displays strong vertical stratification (Fig. 2, left panels). The densest waters are located in the bottom layer, below the SCG (Fig 2c). Circulation in the bottom layer is weak and largely isolated from the PS. A small amount of the GSJ's waters are returned to the PS in a thin Ekman layer but the bulk of the outflow occurs near the northern portion of the mouth (Fig. 3b). Outflowing waters are lighter than those over the PS, thus generating an outflowing jet with a highly baroclinic structure (Suppl. Fig. A). The total volume exchange with the shelf is ~12 cSv (1 cSv = $1x10^4$ m^3/s) and it is dominated by the dynamics of the intermediate layer, where the largest inflows and outflows are compensated (Fig. 3b).

Fall strengthening of wind forcing and weakening of density stratification dampens the cyclonic circulation, replacing it with several anticyclonic gyres (Fig. 2e). During this period the CCC is replaced by a southward flowing coastal current. The SCG and the SEAG weaken but while the former contracts the latter expands, blocking a large portion of the mouth, thus shifting the inflow of PS waters to the north and forming the Northern Loop Current (NLC, Fig. 2e). The transport and inshore penetration of the NLC is weaker than the SLC but its influence extends to the bottom layer, reaching the entire western coast (Fig. 2f). The subsurface portion of the NLC carries relatively denser waters that mix with lighter waters from the south and exit through the north (Fig. 3c). In the deeper portions of the gulf the SCG recirculates remnants of dense water. Lighter waters supplied by the Magellan Strait outflow are confined to the SEAG extension, particularly in its southern well-mixed sector (Fig. 2f). Net exchange with the PS is larger in the intermediate layer and confined to the northern region (Fig. 3c).

Winter convection homogenizes GSJ waters and weakens its circulation (Figs. 2g to 2i). During this season diluted horizontal density gradients remain offshore along the southern coast. In the interior, there is a feeble (~ 0.15 cm/s) northeastward surface flow that creates an open cyclonic loop in the intermediate layer in the north and a broad anticyclonic loop in the south (Fig. 2h). The southern anticyclone splits into two gyres separated by a weak cyclonic structure south of the CB. The cross-shelf exchange with the shelf is at a minimum with comparable contributions from the intermediate and bottom layers (Fig. 3d). A large part of the (lighter) shelf waters recirculates to the east of the mouth over most of the water column as part of an extended SEAG (Fig. 2h).

During spring, the Patagonian Current intensifies and moves inshore, increasing its penetration into the GSJ (Figs. 2k and l). This inflow is concentrated in the intermediate layer, between a broad and shallow NLC and a narrow and deeper SLC. These currents extend over the entire width of the GSJ, encompassing a large portion of the water column (Fig. 3e and Suppl. Fig. A, panel h). The NLC

waters are relatively dense, particularly in the bottom layer (Fig. 2l). The SLC carries lighter waters and loops to the south before heading toward the coast to join the SCG. Spring also marks the start of re-stratification and intensification of cyclonic circulation over the CB, and weakening of the anticyclonic coastal gyres inside the GSJ. Spring exchanges with the PS also increase (Fig 3e).

3.2. Water mass exchanges

We used passive tracers to identify preferential sites of mass exchange and their associated time scales. After the initial release, tracer concentration is controlled by an advection/diffusion equation similar to that used for temperature and salinity:

$$\frac{\partial C}{\partial t} + \nabla \cdot (C\mathbf{u}) = \frac{\partial}{\partial z}\left(K_c \frac{\partial C}{\partial z} \right) + \frac{1}{T_s}(C - C_o) \qquad (1)$$

where C is the tracer's concentration, $\mathbf{u}$ is the ocean velocity field, K_c is a vertical diffusivity coefficient (computed with a two-equation turbulence model), C_o is the tracer's initial concentration and T_s a relaxation time scale.

We conducted three tracer releases. In the first experiment the portion of the GSJ west of 66ºW was initially filled with a tracer of concentration C_o = 1 (T_GSJ). The source term (last term in Eq. 1) is zero, therefore the initial concentration can only decay with time. Hence, the residence time of T_GSJ is calculated at each grid volume of GSJ as the time it takes until the tracer concentration C drops below 37% of the initial value (100%) locally. To account for seasonal differences in circulation T_GSJ was released in December and June, representing summer and winter conditions. The second and third tracers were injected continuously in the PS at a zonal cross-section to the south of Cape Tres Puntas both inshore (T_COA) and offshore (T_OFF) of the 90m isobath (Figs. 6a and c); its subsequent evolution was monitored during a five-year period. In contrast to tracer T_GSJ, a source term (Ts ~ 1day) keeps T_COA and T_OFF at unit concentration (C =1) in the

release areas at all times. In these experiments GSJ is initially void of tracers. Renewal times were computed as the time until the tracer concentration exceeded 67% locally. Since there were no tracer sources inside GSJ, tracer concentrations could only increase with time (owing to continual inflow of tracers through the mouth) and eventually the 67% renewal threshold was exceeded everywhere. Partitioning of shelf tracers in T_COA and T_OFF was dictated by characteristics of the shelf circulation (see Fig. 1c). T_COA represents the source of coastal waters entrained into GSJ while T_OFF is associated with the core of the Patagonian Current. To illustrate their depth dependence, the spatial and temporal evolution of the tracers was vertically averaged in the three layers defined in Fig. 2. For the sake of clarity only the surface and bottom layer concentrations are shown. The tracer distribution in the intermediate layer is similar to the surface layer.

Tracer T_GSJ shows that summer stratification decouples circulation of the surface and bottom layers (Fig. 4a and 4b). By the end of this season (April) most of the surface waters ($z < 15$m) have flowed out onto the shelf through the northern region. Tracer concentrations in the southern region are low except near the southwestern coast. Residence time is less than 60 days in the south and increases towards the north, where patches with residence times longer than 150 days are found (Fig. 4c). Stratification prevents the upwelling and mixing of deep waters ($z > 60$m) (Fig. 4b), whose residence times are larger than 150 days, except in the southwestern coastal zone where the bottom tracer is rapidly brought to the surface by wind-driven upwelling and tidal mixing (Fig. 4d). This result is in agreement with recent hydrographic surveys (Temperoni et al., 2018) and satellite sea surface temperature analysis (Glembocki et al., 2015; Pisoni et al., 2018), which reveal the presence of relatively cold waters at the surface in summer.

Winter convection couples the circulation of surface and deep layers (Fig. 4, bottom panels). T_GSJ has a relatively large residence time (> 150 days), although its concentration is slowly diluted by intrusions of PS waters, mostly in the northern region. These waters, however, do not reach the

coast during the simulation time. The long time it takes to replace GSJ's waters with PS waters indicates that most renewal of GSJ's deep waters (particularly on the CB) is driven by winter convection.

Comparison of tracer plumes reveals that T_COA, which characterizes the inner shelf portion of the Patagonian Current, has the largest influence on the GSJ, particularly during summer (Fig 5a and b). Tracer T_OFF, however, has a substantially smaller penetration into the gulf (Fig. 5d). Its largest intrusions occur in summer at the bottom and are confined to the northern portion of the mouth (Fig. 5e). Smaller intrusions of T_OFF in the southern region form a narrow and elongated tongue that enters the gulf after negotiating the SB. During winter T_COA splits into two branches at the surface layer. The left branch, mainly composed of summer and fall remnants, retracts towards the southeast while the right branch extends to the north with reduced communication with the gulf (Fig 5c). The winter distribution of T_OFF indicates a stronger intrusion in the northern region (Fig. 5f). Because the tracer is vertically homogenized by winter convection the bottom distribution of T_COA and T_OFF (not shown) are similar to the surface patterns.

To visualize the temporal evolution of cross-shelf exchanges we mapped the time it took for each of the PS tracers to replace 63% of GSJ waters (e-folding renewal time) (Fig. 6). Renewal time of T_COA is shorter (< 6 months) in the southeastern region of the GSJ, both in surface and bottom layers. Renewal time increases from less than six months in the southeast to more than three years in the northwest (Fig. 6a and b). T_OFF replaces bottom and surface waters in less than one year in the northern sector, but takes longer in the southern region (Fig. 6c and d). To investigate the contribution of seasonal variability to water mass exchanges we computed the temporal evolution of average tracer concentration in the southern (south of 46ºS) and northern regions (Fig. 7). The southern region, which is mostly influenced by T_COA, displays important seasonal variations in the surface layer (Fig. 7a). Tracer intrusions increase during summer and decrease toward the fall.

Seasonal variations of T_OFF are out of phase with T_COA, exhibiting a maximum in fall and a minimum in spring. The vertical concentration of T_OFF is more uniform than T_COA. In contrast, with the exception of the surface layer in summer, T_OFF dominates the tracer concentration in the northern region, particularly in the bottom layer where the intrusions of offshore waters are even larger than at the surface (Fig. 7b). Seasonal out of phase variations are also evident in the surface layer with T_COA prevailing in summer and T_OFF in winter.

To summarize, during summer the inner portion of the Patagonian Current replenishes most of the surface and intermediate layers of the GSJ. The bottom layer is replaced by local and PS waters in the southern region. In the northern region the PS is the dominant supplier of bottom waters. During winter PS waters prevail in the northern portion of the basin and the intrusion of inner shelf waters is restricted to the southeastern coast.

The GSJ is the second most productive Argentinean hydrocarbon basin. Oil drilling in this basin has been largely confined to onshore regions but steady growth in offshore exploration has significantly increased the risk of oil spills in gulf waters. Modelling oil transport in the marine environment can be quite complex owing to numerous chemical factors that impact its buoyancy (Reed et al., 1999). However, time scales relevant to neutrally buoyant particles or passive tracers can reveal information about the dominant transport time scales that would be expected in the event of an oil spill. Our previous estimates of residence times are not particularly suitable for these purposes because they are computed from the 3-D velocity fields, while oil spills—due to their physical characteristics—are largely constrained to surface layers. To address these matters we characterized the migration pathways and residence times of surface waters. We released 21,700 particles in the surface layers of the region west of 66˚W in January and July, which represent summer and winter circulation conditions. Particle trajectories were calculated off-line (Batchelder, 2006) using only ocean surface velocities. The final distributions of these releases reflect seasonal changes in the

gulf's circulation, and have important implications for coastal ecosystems (Fig. 8a and 8b). Our calculation suggests that oil spills during the summer season would be more detrimental to the ecosystems of the northern portion of the gulf because they are characterized by higher particle concentrations and longer residence times. Outside the gulf, summer oil spills will have a larger impact on nearshore regions of the Patagonian coast while winter spills are more likely to impact shelf ecosystems. Overall, e-folding residence times are 46.5 days for the summer release and 56.6 days for the winter release (Fig. 8c).

4. Circulation drivers

To identify circulation drivers we analyzed two suites of process-oriented experiments: barotropic experiments forced with tides and winds, and stratified experiments forced with different combinations of surface and boundary conditions. Table I lists the general characteristics of these experiments.

4.1. Tides and winds

The tidally-driven circulation in the PS has been previously described, but using lower resolution models than ours (Glorioso and Flather, 1994; Simionato et al., 2004; Palma et al., 2004b). We extend those studies to identify the contribution of tides to bottom friction, vertical mixing and residual circulation in GSJ. We began the analysis with the barotropic experiment EXPNS_T that was forced with the M_2 tidal harmonic, the dominant tidal constituent of this region.

The M_2 tide propagates northward over the PS; near the southern tip of the GSJ it undergoes large phase changes associated with an amphidromic point located farther offshore (Palma et al., 2004b). Within the GSJ tidal amplitudes increase by ~50 cm, reaching a maximum value of 2.00 m close to Comodoro Rivadavia (Fig. 9a). The tidal wave generates a northward energy flux of 36.2 GW

(1GW = $1x10^9$ W). After crossing Cape Tres Puntas one-third of this energy flux (12.6 GW) is lost to bottom friction; the remainder enters the basin and develops a clockwise gyre (Fig. 9b). The interaction of strong tidal currents (> 1.5 m/s, not shown) with the bottom topography generates dissipation rates (> 2.5 W/m^2) that are among the largest in the PS (Palma et al., 2004b). These values suggest that tidally driven turbulence, which increases bottom stress and vertical mixing, should have substantial influence on the GSJ's hydrodynamics. Since tidal currents are larger than mean flows most of the dissipation can be attributed to the tides.

EXPNS_W and EXPNS_TW assessed the impact of tides on the time mean circulation (Fig. 9c and 9d). The former was only forced with annual mean winds and the latter with tides and winds. Wind forcing on EXPNS_W is not restricted to the interior of the GSJ but also encompasses the PS, where it generates a strong northward current that enters the gulf. To isolate the effect of winds on EXPNS_TW we computed the difference between EXPNS_TW and EXPNS_T (Fig. 9d). The tidally induced increment of bottom friction in EXPNS_TW generates substantial changes in EXPNS_W. These changes are not only quantitative (weaker flows) but also qualitative. In the southern region, for example, the cylonic meander is replaced by a wide anticyclonic gyre. A depth-averaged steady-state vorticity balance indicates that the two-gyre structure shown in Fig. 9d is generated by the interaction between zonal wind forcing and the particular geomorphology (coastline and bathymetry) of the GSJ (Matano and Palma, 2018).

EXPS_T and EXPS_TW evaluated the impact of tidal forcing on vertical mixing and residual circulation. Both experiments were initialized with January area-averaged temperature and salinity profiles, i.e., at the initial state T= T(z) and S= S(z) only (Figs. 11 a and b). EXPS_T was forced only with the M_2 tide and EXPS_TW with tides and winds. Atmospheric fluxes (heat and salt) wer held constant through relaxation to the initial surface values of T and S. These experiments were integrated for 120 days. A monthly average of the last 30 days is used in the following discussion.

The Simpson parameter, Φ_c (Simpson, 1981), which represents the energy needed to homogenize a stratified water column, characterizes the impact of tides on vertical mixing. Values of $\Phi_c < 40$ J/m^3, which represent homogenous conditions in this region (Sabatini and Martos, 2002), are found in the southern sector of GSJ as well as the coastal areas and the region near Cape Dos Bahías (Fig. 10a). Critical contours computed with hydrographic data (Temperoni et al., 2018) agree very well with model results. Note also the spatial agreement between the regions delimited by the critical contour and maximum tidal dissipation (Fig. 9b).

The non-linear interaction of the tidal wave with bottom topography and stratification generates time-averaged residual currents. The barotropic experiment EXPNS-T shows a large and elongated anticyclonic gyre centered close to 46°S with an intense NE jet to the right of the SB and slower southward flowing coastal currents. Smaller circulation structures near the northern and southern tips of the mouth form cyclonic/anticyclonic recirculating vortices (Fig. 10b). As shown in previous work these patterns are driven by the non-linear advection of vorticity associated with differential friction and bottom torque (Tonini and Palma, 2017; Matano and Palma, 2018).

Inclusion of density stratification in EXPS-T alters the residual circulation patterns described above (Fig. 10c). An intensified northward flowing inner shelf current turns to the west after negotiating the SB and joins the CCC. The southern portion of this current is narrow and strong, while the northern portion widens and gradually leaks into the interior. A small recirculating cyclonic gyre is also visible over the CB. Similarities with the barotropic solution are restricted to the two anticylonic gyres over the SB (SEAG) and Camarones Bay, which are the locations with largest tidal mixing (Fig. 10a). The cyclonic coastal current in EXPS-T is driven by differential tidal mixing in shallow coastal areas and deeper central regions, generating a density front and geostrophic jets (Fig. 11, middle panels; Aretxabaleta et al., 2008). Isopycnals in the southern

section are perpendicular to the bottom near the coast and close to the mouth. The velocity field exhibits a deep and narrow jet nearshore and a weak cyclonic gyre surrounding the dome of high density water over the CB (Fig. 11c). The east (southward flowing) branch of the gyre is enhanced by the intrusion of the shelf current after circling the SB. Similar baroclinic frontal structures generated by tidal forcing have been reported in Georges Bank (Lough and Manning, 2001) and the Irish Sea (Horsburgh et al., 2000). The coastal density distribution in the northern section shows a similar density structure with weaker gradients (possible due to the gentler topographic gradient here) and the resulting geostrophic jet is broader and weaker (Fig 11d). It is also possible that the smooth topographic transition between the GSJ's interior and the PS (compared with the southern sector) prevents the formation of a recirculating gyre in the northern sector.

EXPS-TW shows the contribution of wind forcing to GSJ circulation, which is particularly important in coastal areas and the northern region (Figs. 10d). Intensification of the shelf circulation leads to a larger intrusion of shelf waters into the GSJ north of 46ºS. These waters join a broad northward flowing current that is absent in EXPS-T. Near the coast the wind generates an elongated anticyclonic gyre that covers a large part of the gulf, thus weakening and/or inverting the coastal current shown in EXPS-T. Wind forcing also modifies the nearshore vertical structure of the density and velocity fields (Fig. 11, bottom panels). In the southern sector intense coastal upwelling induces upward tilt of the surface and intermediate layer (< 50 m) isopycnals with an associated geostrophic southward flowing coastal jet (Fig. 11e). Relatively cold surface waters in summer, indicative of upwelling, have been detected in this region both in hydrographic surveys (Temperoni et al., 2018) and satellite imagery (Glembocki et al., 2015; Pisoni et al., 2018). Offshore there is a well-defined vertically homogenous Ekman layer (~20m thick) with northward flowing currents. The southward flowing branch of the intruding shelf current (to the left of the SB) appears to also be enhanced by the wind. In the northern sector the coastal isopycnals begin to bend upward deeper in the water column, hence the core of the geostrophic (southward) coastal current migrates to the subsurface

layer (Fig. 11f). Consequently a weak and broad CCC, boosted at the surface by wind-driven currents, persists at this location (Fig. 10d). In summary, tides and winds acting locally on a weakly stratified GSJ basin generate a 3-D circulation with substantial similarities to the spring and summer solution of the BENCH experiment.

4.2. Seasonal variability

To investigate the impact of seasonal variation of forcing on the circulation we ran EXPSS-T, which is initialized as BENCH but run without wind forcing. EXPSS-T (February) exhibits circulation patterns similar to EXPS-T but more intense (Fig. 10c and Fig. 12a). The intensity increment could be caused by remote forcing (through Drake Passage) and/or stronger stratification generated by larger surface heat fluxes in February as compared with the average fluxes of EXPS-T (compare Fig. 11, middle panels and Fig. 13, top panels). It is difficult, however, to separate the contributions of the different drivers since heat fluxes enhance PS stratification and hence the baroclinic contribution of remote forcing. In May negative atmospheric heat fluxes reduce vertical stratification, weakening the CCC and the SCG (Fig. 12b). By August the water column is completely homogenized by vertical convection and, with the exception of a weak cyclonic gyre in the southern region, the tidally induced circulation inside the GSJ is anticyclonic and similar to the barotropic case (Figs. 12c and Fig. 10b). We ascribe the cyclonic recirculation to horizontal density gradients associated with intrusions of the inshore branch of the Patagonian Current (Fig. 5c). In November the surface heat fluxes are again into the ocean and the seasonal cycle of re-stratification begins with a consequent intensification of a GSJ-wide cyclonic circulation (Fig. 12d). Note that the well mixed areas near the SB and Camarones Bay are occupied year-long by anticyclonic gyres generated by topographic tidal rectification (Fig. 10b).

To assess the contribution of seasonal variation in wind forcing to the gulf's circulation we compared EXPSS-T and BENCH (Fig. 12). There are no substantial seasonal changes in wind

direction but wind speed is stronger during fall and weaker during spring (not shown). The wind-induced changes during the summer and spring seasons are very similar to those discussed in section 4.1 (EXPS-TW, area-averaged initial stratification and annual mean wind forcing) particularly in spring (Fig. 10d and Fig. 12h): stronger PS currents, weaker CCC and a more energetic and organized circulation pattern in the northern region. The strong northward flow that develops just outside the gulf's mouth during summer is partly associated with Ekman dynamics but mostly driven by the formation of a strong subsurface baroclinic frontal jet that is absent in the tidal only solution (~66.5ºW, Fig. 13b and d). Weakening of the CCC is caused by coastal upwelling, which generates a southward flow. During spring, coastal upwelling inverts the coastal flow in the southern region (Fig. 12h and Fig. 13g). In summer, however, the cyclonic circulation generated by the interaction of strong stratification and tidal forcing overwhelms the wind action and a well-defined northward coastal jet persists (Fig. 12e and Fig. 13c).

During fall and winter, when vertical stratification weakens, the depth-averaged circulation is further modified by wind forcing. In the southern region the tidally-induced cyclonic circulation is replaced by anticyclonic patterns, the exception being the region over the CB. In the northern region, large zonal intrusions of the offshore portion of the Patagonian Current develop cyclonic circulation loops. Additionally, the area spanned by the anticyclonic gyre over the SB, whose existence is related to topographic (tidal) rectification, displays a meridional elongation under wind forcing (Fig. 12f and g).

5. Summary and final remarks

During late spring and summer the GSJ circulation is mostly cyclonic and composed of a narrow, gulf-wide coastal current and a re-circulating gyre in the southern region. Stratification decouples the circulation of upper and deep layers, leading to a shallow surface Ekman-type circulation and a

subsurface, density driven, geostrophic flow. These patterns are replaced during fall and winter by anticyclonic gyres in the coastal region and an open cyclonic loop in the north.

Sensitivity experiments indicate that the GSJ circulation is mainly shaped by the interaction of tidal forcing with density stratification and modulated by wind forcing and intrusions from the PS. PS currents are driven by density gradients shaped by tidal and wind forcing and also by ACC intrusions at the Drake Passage (Palma et al., 2008; Combes and Matano, 2018). Note, however, that once the open boundary fluxes are turned on it is no longer possible to properly separate the remote (baroclinic) contributions of the ACC from those driven by tides and winds. The presence of a strong coastal current during summer is related to differential tidal mixing in coastal and deep areas and the consequent development of horizontal density gradients. Wind forcing promotes uplift of isopycnals near the coast and a southward coastal current. The direction of this current varies seasonally. In summer it is mostly cyclonic but it gradually wanes towards fall and winter, when it is replaced by anticyclonic gyres. Even in fall and winter however, the northern portion of the GSJ is dominated by northward, mostly wind-driven coastal currents. Model results also suggest that the SCG is driven by tidal forcing but its spatial extent and intensity are strongly affected by the temporal variability of atmospheric forcing. The SCG strengthens from spring to summer and fades from fall to winter. The permanent anticyclonic gyre (SEAG) located over the SB is generated by tidal rectification although its meridional extension and intensity appear to be regulated by seasonal changes in the magnitude and location of the intruding PS currents and wind forcing.

Passive tracers identify the preferential sites of cross-shelf exchanges and the characteristics of those exchanges. In summer, GSJ exports surface and subsurface waters from its northern coast and replaces them with waters mostly derived from the inner (coastal) portion of the Patagonian Current. The renewal of bottom waters is slower. A small portion upwells in the southwestern coast where it is flushed out by surface currents. The bulk of the bottom waters, however, are ventilated

later through winter convection in the south and by intrusions of PS waters in the northern region. Particle trajectories driven by surface horizontal currents indicate that an oil spill in summer would be more detrimental to the ecosystems of the northern portion of the gulf and would have a larger impact on the nearshore regions of the Patagonian coast. Winter spills are more likely to impact the region close to the mouth and the ecosystems on the outer shelf.

Observational data to develop a systematic quantitative validation of the climatological circulation patterns presented here do not exist. For a qualitative evaluation of the model's realism, however, we compared model results with temperature data collected in January 1995 and 2006 by the Argentinean Institute of Fisheries (INIDEP, Baldoni et al., 2008) at two selected cross-sections. The observed temperature field at the mouth (C1, Fig. 1b) shows three well defined regions that are reproduced by the model: a southern sector, which is characterized by a well-mixed and relatively warm water mass structure, a northern sector (north of ~46.3ºS), which is strongly stratified and includes a relatively deep mixed layer, and a central sector, which is weakly stratified and colder than the southern sector (Fig. 14a and c). Since density plays a prominent role in intensification of the summer cyclonic circulation (i.e., the CCC and SCG) we also compared a section transversing the CB (C4, Fig.1b). Field data and model results show a doming of isotherms, with colder waters over the deeper parts bending downward near the coast and close to the SB, in response to the intense vertical mixing induced by tidal currents (Fig. 14b and d). A major difference between model results and observations is the thermocline depth, which is ~15m deeper in the latter. The difference appears to be related to climatological wind forcing in the model, as ancillary experiments forced with daily winds produce deeper thermoclines (Fig. 14, bottom panels). These effects will be more thoroughly discussed in a forthcoming study.

Circulation patterns similar to those described herein have been reported in other gulfs and bays of the world ocean. Xue et al. (2000) reported a summer intensification of coastal circulation in the

Gulf of Maine, attributing it to the combination of differential heating of coastal (warmer) and offshore (cooler) areas and intense tidal mixing. A similar physical mechanism, associated with topographically induced horizontal gradients in tidal mixing and the subsequent generation of frontal structures in the density field has been invoked by Arexabaleta et al. (2008) to explain the Bay of Fundy gyre. Tidal mixing over banks forces down isopycnals in deep layers generating an upper layer cyclonic circulation (Hill, 1993). Summer intensified cyclonic recirculating patterns like the SCG are expected if a cold water pool produced by winter convection is isolated by tidal mixing during the start of stratification (Fig. 14, right panels). Similar cyclonic recirculating patterns associated with dense bottom lenses have been observed and modeled in the Gulf of California (Lavin et al., 1997), the Yellow Sea (Naimie et al., 1994), the Irish Sea (Hill et al., 1997) and the Argentinean North Patagonian Gulfs (Tonini et al., 2013). Conversely, the main anticyclonic gyres (southwestern and southeastern) are mostly barotropic in nature although driven by distinct forcing mechanisms. The southeastern gyre is developed by the mechanism of barotropic tidal rectification over the SB while the southwestern gyre is generated by the westerly winds acting on the particular geomorphology of the GSJ. These results are consistent with similar barotropic models of the Patagonian Shelf (Tonini and Palma, 2017; Tonini et al., 2006; Palma et al., 2004b).

6. Acknowledgments

E.D. Palma and M. H. Tonini acknowledges financial support from Agencia Nacional de Promoción Científica y Tecnológica (grant PICT16-0557) and Universidad Nacional del Sur (grant 24F079), Argentina. R. Matano and V. Combes acknowledge NASA support through grant NNX17AH20G and the National Science Foundation through grants OCE-1357530 and OCE-1559550. M. H. Tonini also acknowledges financial support from Subsidio Pampa Azul (Grupo de Trabajo Golfo San Jorge, MINCYT 036/16). P. Martos acknowledges financial support from INIDEP and technical support from H. Fenco. SeaWiFS data (Fig. 1a) is from NASA Ocean Color

Group (https://oceancolor.gsfc.nasa.gov). Hydrographic data (Fig. 14) is stored in Base Regional de Datos Oceanográficos (BaRDO)-INIDEP.

6. References

Arexabaleta A., D. J. McGillicuddy Jr., K. W. Smith, and D. R. Lynch. 2008. Model simulations of the Bay of Fundy Gyre: 1. Climatological results, *J. Geophys. Res. Oceans*, 113, C10027,1-16.

Barnier, B. 1998. Forcing the ocean, in *Ocean Modelling and Parameterization*. E. P. Chassingnet and J. Verron, eds, Kluwer Academic Publishers, The Netherlands, 45-80.

Baldoni, A., Molinari, G., Guerrero, R. A., and M. Kruk. 2008. Base Regional de Datos Oceanográficos (BaRDO) INIDEP. *Informe de Investigación INIDEP*, 13, 1-25.

Batchelder, H. 2006. Forward-in-Time-/Backward-in-Time-Trajectory (FITT/BITT) Modeling of Particles and Organisms in the Coastal Ocean, *J. of Phys. Oceanogr.*, 36, 727-741

Bogazzi, E., A. Baldoni, A. Rivas, P. Martos, R. Reta, J. M. Orensanz, M. Lasta, P. Dell'Arciprete, and F. Werner. 2005. Spatial correspondence between areas of concentration of Patagonian scallop (*Zygochlamys patagonica*) and frontal systems in the southwestern Atlantic. *Fish. Oceanogr.* 14,359-376.

Combes, V. and Matano, R.P., 2014a. A two-way nested simulation of the oceanic circulation in the Southwestern Atlantic. *J. Geophys.Res.: Oceans*, 119(2), 731-756.

Combes, V. and Matano, R.P., 2014b. Trends in the Brazil/Malvinas confluence region. *Geophys. Res. Letters*, 41(24), 8971-8977.

Combes, V. and Matano, R.P., 2018. The Patagonian shelf circulation: Drivers and variability. *Progress in oceanography*, 167, 24-43.

Conkright, M.E., R. A. Locarnini, H. E. Garcia, T. D. OBrien, T. P. Boyer, C. Stephens, and J. I. Antonov. 2002. *World Ocean Atlas 2001: Objective Analyses, Data Statistics, and Figures*. National Oceanographic Data Center. Silver Spring, MD, CD-ROM Documentation 17 pp.

Da Silva, A. M., C. C. Young, and S. Levitus. 1994. *Atlas of Surface Marine Data 1994*, vol. 1, Algorithms and Procedures, NOAA Atlas NESDIS 8, 83 pp., U. S. Dep. of Commer., NOAA, NESDIS, Washington, D. C.

Debreu, L., P. Marchesiello, P. Penven, and G. Cambon. 2011. Two-way nesting in split-explicit ocean models: Algorithms, implementation and validation, *Ocean Modell*., 49-50, 1–21.

De la Garza, J., Moriondo Danovaro, P., Fernandez, M, Ravalli, C., Souto, V., and J.Waessle, J. 2017. An overview of the Argentine red shrimp (*Pleoticus muelleri*, Decapoda, Solenoceridae) fishery in Argentina. Biology, fishing, management and ecological interactions. 42 pp. Instituto Nacional de Investigacion y Desarrollo Pesquero INIDEP, N° 2080, Mar del Plata, Argentina.

Egbert, G. D., A. F. Bennett and M. G. Foreman. 1994. Topex/Poseidon tides estimated using a global inverse model. *J. Geophy. Res., Oceans,* 99, 24821-24852.

Glembocki, N. G., G. N. Williams, M. E. Góngora, D. A. Gagliardini and J. M. Orensanz. 2015. Synoptic oceanography of San Jorge Gulf (Argentina): A template for Patagonian red shrimp (Pleoticus muelleri) spatial dynamics, *J. Sea Res.,* 95, 22-35.

Glorioso, P. D., and R. A. Flather. 1995. A barotropic model of the currents off SE South America, *J. Geophys. Res., Oceans* 100, 13,427–13,440.

Hill, A. E.. 1993. Seasonal gyres in shelf seas, *Ann. Geophys*., 11, 1130– 1137.

Hill, A.E., J. Brown, and L. Fernand.1997.The summer gyre in the Western Irish Sea: shelf Sea paradigms and management implications. *Estuar., Coast. Shelf Sci.*, 44A, 83–95.

Horsburgh, K. J., A. E. Hill, J. Brown, L. Fernand, R. W. Garvine, and M. M. P. Angelico. 2000. Seasonal evolution of the cool pool gyre in the western Irish Sea, *Prog. Oceanogr*., 46, 1– 58.

Hu, D., M. Cui, y. Li, and T. Qu. 1991. On the Yellow Sea cold water mass related circulation. *Yellow Sea Research*, 4, 79–88.

Krock, B., C. M. Borel, F. Barrera, U. Tillmann, E. Fabro, G. O. Almandoz, M. Ferrairo, J. E. Garzón Cardona, B. P. Koch, C. Alonso and others. 2015. Analysis of the hydrographic conditions

and cyst beds in the San Jorge Gulf, Argentina, that favor dinoflagellate population development including toxigenic species and their toxins. *J. Mar. Syst.,* 148, 86–100.

Large, W., J. McWilliams, and S. Doney. 1994. Oceanic vertical mixing—A review and a model with a nonlocal boundary-layer parameterization. *Rev. Geophys.,* 32(4), 363–403.

Lavin, M.F., R. Durazo, E. Palacios, M. L. Argote, and L. Carrillo.1997. Lagrangian observations of the circulation in the Northern Gulf of California. *J. Phys. Oceanogr.,* 27, 2298–2305.

Lough, R. G., and J. Manning. 2001. Tidal-front entrainment and retention of fish larvae on the southern flank of Georges Bank, *Deep Sea Res., Part II*, 48, 631– 644.

Marrari M, Piola AR and Valla D. 2017. Variability and 20-Year Trends in Satellite-Derived Surface Chlorophyll Concentrations in Large Marine Ecosystems around South and Western Central America. *Front. Mar. Sci*. 4:372. doi: 10.3389/fmars.2017.00372.

Marchesiello, P., J. C. McWilliams, and A. Shchepetkin. 2001. Open boundary conditions for long-term integration of regional oceanic models. *Ocean Modell.,* 3,1–20.

Matano, R.P., Combes, V., Piola, A.R., Guerrero, R., Palma, E.D., Strub, P.T., James, C., Fenco, H., Chao, Y. and Saraceno, M., 2014. The salinity signature of the cross-shelf exchanges in the Southwestern Atlantic Ocean: Numerical simulations. *J. Geophys. Res., Oceans*, 119(11), 7949-7968.

Matano R. P. and E. D. Palma. 2018. Seasonal Variability of the Oceanic Circulation in the Gulf of San Jorge, Argentina. *Oceanography*, 31(4), 16-24.

Naimie, C. E., C. A. Blain and D. R. Lynch. 1994. Seasonal mean circulation in the yellow Sea – a model-generated climatology. *Cont. Shelf Res*., 21, 667-695.

Palma, E.D., R. P. Matano, A. R. Piola and L. Sitz . 2004a. A comparison of the circulation patterns over the Southwestern Atlantic driven by different wind stress climatologies. *Geophys. Res. Lett.* Vol 31, L24303, doi:10.1029/2004GL021068.

Palma, E. D., R. P. Matano, and A. R. Piola. 2004b. A numerical study of the Southwestern Atlantic Shelf circulation: Barotropic response to tidal and wind forcing. *J. Geophys. Res., Oceans* 109, C08014, doi:10.1029/2004JC002315.

Palma E. D., and R. P. Matano. 2012. A Numerical Study of the Magellan Plume. *J. Geophys. Res., Oceans* 117, C05041, doi:10.1029/2011JC007750.

Silwan, C. A . 2001. Geology of the Golfo San Jorge Basin, Argentina, *Journal of Iberian Geology,* 27, 123-157.

Pisoni, J. P., Rivas, A. L., and M. H. Tonini. 2018. Upwelling Costero en el Golfo San Jorge, *X Jornadas Nacionales de Ciencias del Mar*, Buenos Aires, July 30-August 3, 2018, pp. 120.

Reed, M., O. I. Johansen, P. J. Brandvik, P. Daling, A. Lewis, R. Fiocco, D. Mackay, and R. Prentki. 1999. Oil spill modeling towards the close of the 20th century: Overview of the State of the Art, *Spill Sci. Technol. Bull.*, 5(1), 3–16.

Simpson, J.H.,1981. The Shelf-sea fronts: implications of their existence and behavior. *Philosophical Transactions of the Royal Society of London A,* 302, 531–546.

Sabatini, M., and P. Martos. 2002. Mesozooplankton features in a frontal area off northern Patagonia (Argentina) during spring 1995 and 1998. *Scientia Marina*, 66(3), 215-232.

Simionato, C.G., Dragani, W., Nuñez, M. And M. Engel. 2004. A Set of 3-D Nested Models for Tidal Propagation from the Argentinean Continental Shelf to the Río de la Plata Estuary. Part I. M2. *J. Coast. Res*., 20, 641-936.

Strub, P.T., James, C., Combes, V., Matano, R.P., Piola, A.R., Palma, E.D., Saraceno, M., Guerrero, R.A. Fenco, H., L. Etcheverry. 2015. Altimeter-derived seasonal circulation on the southwest Atlantic shelf: 278–438S. *J. Geophys. Res., Oceans, 120,* 3391-3418.

Temperoni, B., A. Massa, C. Derisio, P. Martos, G. Berghoff and M. D. Viñas. 2018. Effect of nursery ground variability on condition of age 0+years Merluccius hubbsi. *J. of Fish Biol*., in press.

Tonini, M. H., E. D. Palma, and A. L. Rivas. 2006. Modelo de alta resolución de los golfos norpatagónicos. *Mecánica Computacional* XXV,1441–1460. http://wwwamcaonline.org.ar.

Tonini, M.H., E. D. Palma and A. R. Piola. 2013. A numerical study of gyres, thermal fronts and seasonal circulation in austral semi-enclosed gulfs. *Cont. Shelf Res.,* 65, 97-110.

Tonini, M.H., and E. D. Palma. 2017. Tidal dynamics on the North Patagonian Argentinean Gulfs. *Estuar., Coast. Shelf Sci..,* 65, 97-110.

Torres A. I., M. Faleschini and J. L. Esteves. 2016. Benthic fluxes and nitrate reduction activity in a marine park (Northern San Jorge Gulf) from Patagonia Argentina. *Environmental Earth Sciences*, 75(815), 1-9.

Xue, H., F. Chai, and N. R. Pettigrew. A model study of the seasonal circulation in the Gulf of Maine. *J. Phys. Oceanogr.*, 30, 1111–1135.

Figure 1. Geographical setting and summer circulation. (a) Model domain showing satellite surface chlorophyll-a concentration (mg/m3) derived from a SeaWiFS 1998-2002 climatology over the PS. Spatial resolution is 9km x 9km. The thin white line indicates the 200m isobath. (b) Insert showing the main geomorphological features of the GSJ. Colours indicate the bottom topography in m. Also shown are the magnitude and direction of the annual mean wind stress vectors. The red dashed lines indicate the position of several transects discussed in the text. C1 = mouth section, C2 = southern section, C3 = northern section and C4 = survey section. (c) Summer depth-mean circulation in GSJ. CCC=cyclonic coastal current, SCG=southern cyclonic gyre, SLC= southern loop current, SEAG=southeastern anticyclonic gyre. Colours indicate velocity magnitude in cm/s.

Figure 2. Seasonal velocity vectors and density fields (colours) (layered averaged). Surface layer (0-15m), Intermediate layer (15-60m), deep layer (60-bottom). The approximate distribution of layer thickness is indicated in Fig. 3a. February (a, b and c), May (d, e, and f), August (g, h and i) and November (j, k , and l). Note the different colorbar for the February density fields.

Figure 3. Cross-shelf transport. (a) Cross-section of density (top panel) at the mouth cross-section (C1, see Fig 1b). Panels (b)-(e) show the unit width transport across the section and averaged in three different vertical layers (the layers are indicated in the top panel). Negative (positive) values indicate transport into (out) the GSJ. Also indicated are the total cross-shelf transport in cSv. Note that panel (d) has a different vertical scale.

Figure 4. GSJ tracers. Monthly averaged concentration (in %, a,b,e,f) and residence time (days, c,d,g,h) for the inner Gulf tracer (T_GSJ) for summer (top panels) and winter (bottom panels) releases. SURFACE =(0-15 m average), BOTTOM = (60-bottom average). The approximate distribution of layer thickness is indicated in Fig. 3a. Note the different colobar scale for concentration and residence time.

Figure 5. Shelf tracers. Monthly averaged concentration (in %) for the inner shelf (T_COA, top panels) and middle shelf (T_OFF, bottom panels) tracers. SURFACE =(0-15 m average), BOTTOM = (60-bottom average). The approximate distribution of layer thickness is indicated in Fig. 3a.The February panels correspond to the third year of simulation; the August panels to the second year.

Figure 6. Shelf tracers. Renewal time (in yrs) for the inner shelf (T_COA, top panels) and middle shelf (T_OFF, bottom panels) tracers. SURFACE =(0-15 m average), BOTTOM = (60-bottom average). The approximate distribution of layer thickness is indicated in Fig. 3a. The red rectangles in panels (c) and (d) indicate the initial position (from surface to bottom) of the shelf tracers.

Figure 7. Shelf tracers. Time series of average concentration of the PS tracers in the southern (< 46°S, top) and northern (bottom) regions of GSJ. T_COA S = surface layer average of the inner shelf tracer, T_COA B = bottom layer concentration, T_OFF S = surface layer concentration of the middle shelf tracer, T_OFF B = bottom layer

concentration. The gray vertical bar indicates the late fall-winter season while the cyan vertical bar corresponds to the late spring-summer period.

Figure 8. Particle's concentration (in particles/100 km^2, a,b) and overall residence time (c) for 21700 particles initially released inside GSJ (longitude < 66W) during January and July in the surface layer (z <-10 m). No vertical advection is allowed in these experiments. The dashed line in (c) indicates the 37% concentration thereshold (e-folding time). Particle's concentration in (a) and (b) are displayed at this time.

Figure 9. Barotropic experiments. (a) M_2 Cotidal chart, amplitude (colours) and phase (white contours), (b) Tidal energy flux (vectors, W/m) and tidal dissipation (colours, W/m^2). White numbers indicate integrated fluxes (GW) across the indicated cross-sections. Red numbers indicate area-integrated dissipation (GW). (c) Depth-averaged velocity vectors and stream-function (colours, in cSv $=10^4$ m^3/s from experiment EXPSNS_W (wind only). (d) Idem as (c) but for the difference between an experiment forced by tides and winds and the other forced by tides only.

Figure 10. Stratified experiments. (a) Simpson Parameter. Values below the critical contour 40 J/m^3 are masked. (b) Monthly and depth-averaged velocity vectors and stream function (colours) from experiment EXPNS_T . (c) Idem for experiment EXPS_T. (d) Idem for EXPS_TW.

Figure 11. Stratified experiments. Zonal cross-sections at a southern (C2, left panels) and northern (C3, right panels) sectors of GSJ (see Fig. 1b) for an experiment forced with tides only (EXPS_T, middle panels) and with tides and winds (EXPS_TW, bottom panels). Colours indicate density and contours velocity normal to the section. White dashed lines indicate negative (i.e. southward) values.

Figure 12. Seasonal evolution of the monthly mean stream function (colours in cSv) and residual (30 day average) depth-mean velocity vectors from the experiments forced with seasonal atmospheric (buoyancy) forcing, tides and remote inflows. Top panels, experiment without winds (EXPSS-T). Bottom panels, BENCH experiment. Thick black lines indicate the zero contour.

Figure 13. Stratified experiments. Zonal cross-sections at a southern (left panels) and northern sectors of GSJ (see Fig. 1b) from the experiments forced with seasonal atmospheric (buoyancy) forcing, tides and remote inflows (EXPSS_T) and BENCH. Colours indicate density and contours velocity normal to the section. White dashed lines indicate negative (i.e. southward) values.

Figure 14. Comparison with observations. Cross-sections of temperature at the Gulf's mouth (section C1, see Fig. 1b, left panels) and at a NW section crossing the CB (section C4, see Fig 1b, right panels). Colours indicate temperature. The horizontal black dashed line indicate the approximate position of the thermocline.

Table I. Characteristics of the numerical experiments described in the text. Sfluxes = Surface fluxes, Bfluxes = Open boundary fluxes.

	Initial Stratification	Forcing	Obs
BENCH	WOA	Tides, Winds, Sfluxes & Bfluxes	Surface and boundary forcing include the annual cycle
EXPSS_T	WOA	Tides, Sfluxes & Bfluxes	No winds
EXPS_T	T(z) & S(z)	Tides, Sfluxes, no Bfluxes	Constant Sfluxes, No winds
EXPS_TW	"	Tides, winds, Sfluxes, no Bfluxes	Constant Sfluxes, annual winds
EXPNS_T	T & S constant	Tides, no Sfluxes or Bfluxes	Barotropic, no winds
EXPNS_W	"	Winds, no Sfluxes or Bfluxes	Barotropic, no tides
EXPNS_TW	"	Tides+winds, no Sfluxes or Bfluxes	Barotropic

Highlights

- Circulation is driven by tides and modulated by winds and intrusions from the PS.
- GSJ export surface and subsurface waters from its northern coast.
- GSJ bottom waters are ventilated mainly by winter convection.

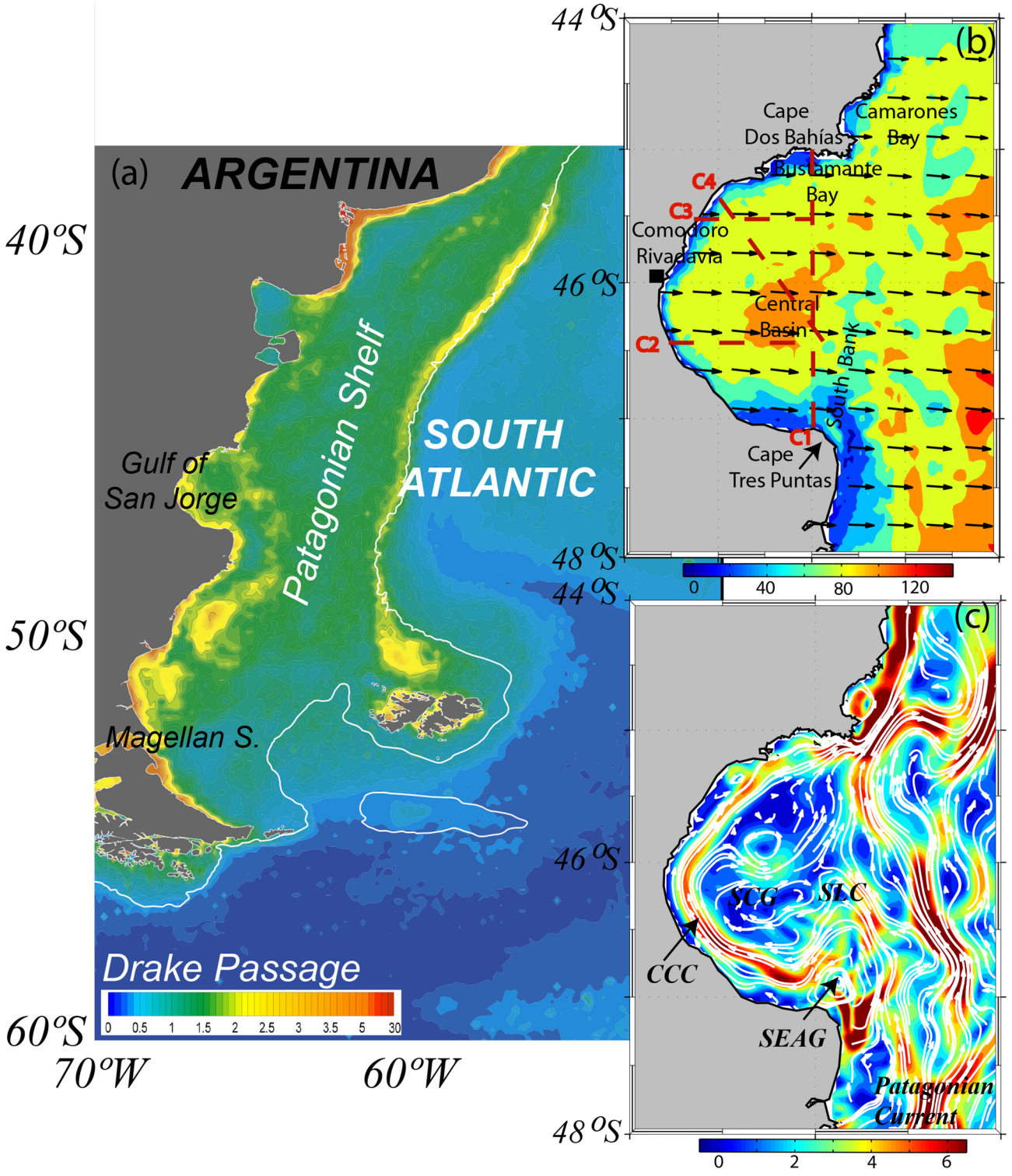
(a)
ARGENTINA
40°S
50°S
60°S
70°W
60°W
Patagonian Shelf
SOUTH ATLANTIC
Gulf of San Jorge
Magellan S.
Drake Passage
0 0.5 1 1.5 2 2.5 3 3.5 5 30
(b)
44°S
46°S
48°S
Cape Dos Bahías
Camarones Bay
Bustamante Bay
C4
C3
C2
C1
Comodoro Rivadavia
Central Basin
South Bank
Cape Tres Puntas
0 40 80 120
(c)
44°S
46°S
48°S
SCG
SLC
CCC
SEAG
Patagonian Current
0 2 4 6

Figure 1

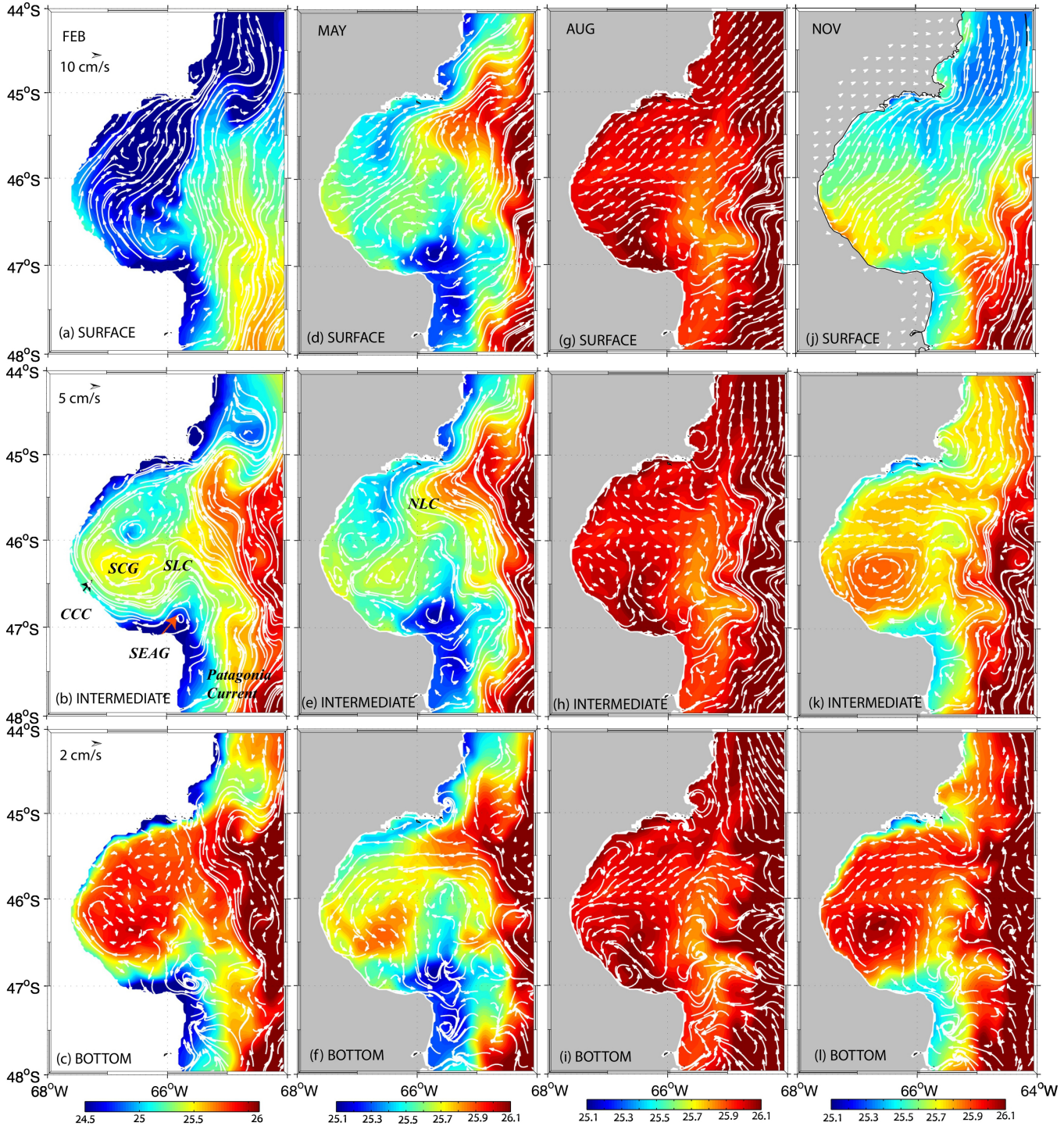
FEB
10 cm/s
MAY
AUG
NOV
(a) SURFACE
(d) SURFACE
(g) SURFACE
(j) SURFACE
5 cm/s
SCG
SLC
CCC
SEAG
Patagonia Current
NLC
(b) INTERMEDIATE
(e) INTERMEDIATE
(h) INTERMEDIATE
(k) INTERMEDIATE
2 cm/s
(c) BOTTOM
(f) BOTTOM
(i) BOTTOM
(l) BOTTOM
44°S
45°S
46°S
47°S
48°S
68°W
66°W
64°W
24.5 25 25.5 26
25.1 25.3 25.5 25.7 25.9 26.1

Figure 2

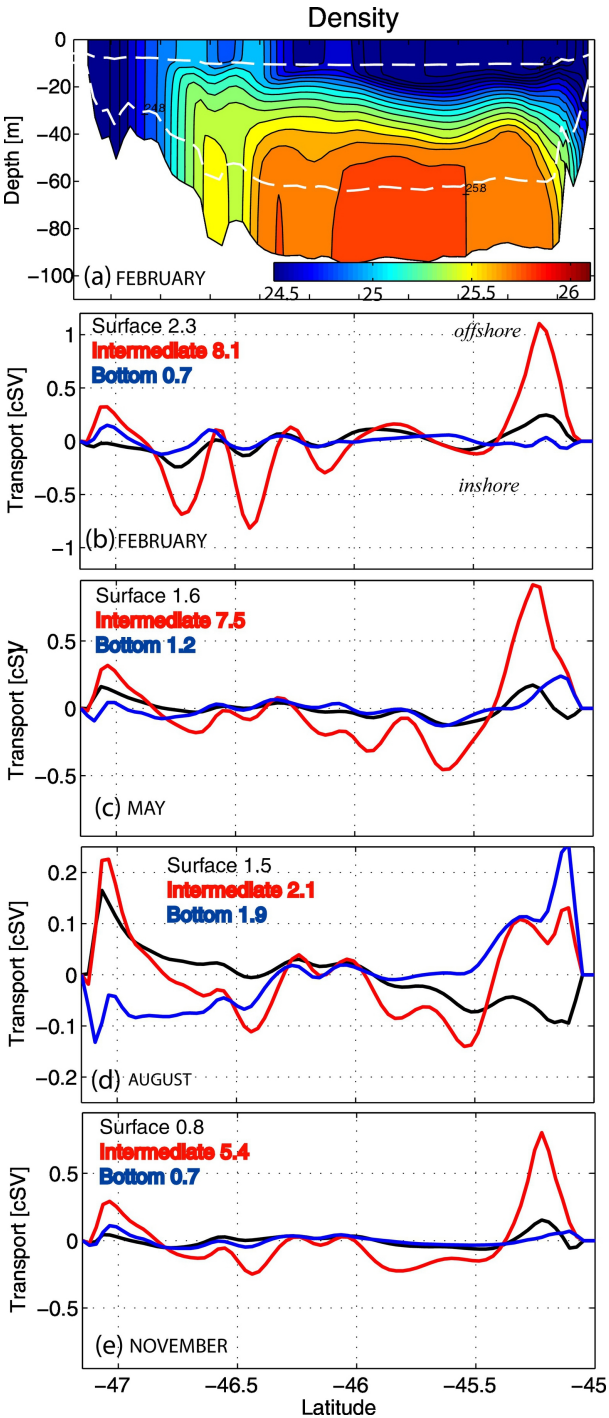
Density
Depth [m]
0
−20
−40
−60
−80
−100
(a) FEBRUARY
24.5
25
25.5
26
Surface 2.3
Intermediate 8.1
Bottom 0.7
offshore
inshore
Transport [cSV]
(b) FEBRUARY
Surface 1.6
Intermediate 7.5
Bottom 1.2
(c) MAY
Surface 1.5
Intermediate 2.1
Bottom 1.9
(d) AUGUST
Surface 0.8
Intermediate 5.4
Bottom 0.7
(e) NOVEMBER
−47
−46.5
−46
−45.5
−45
Latitude

Figure 3

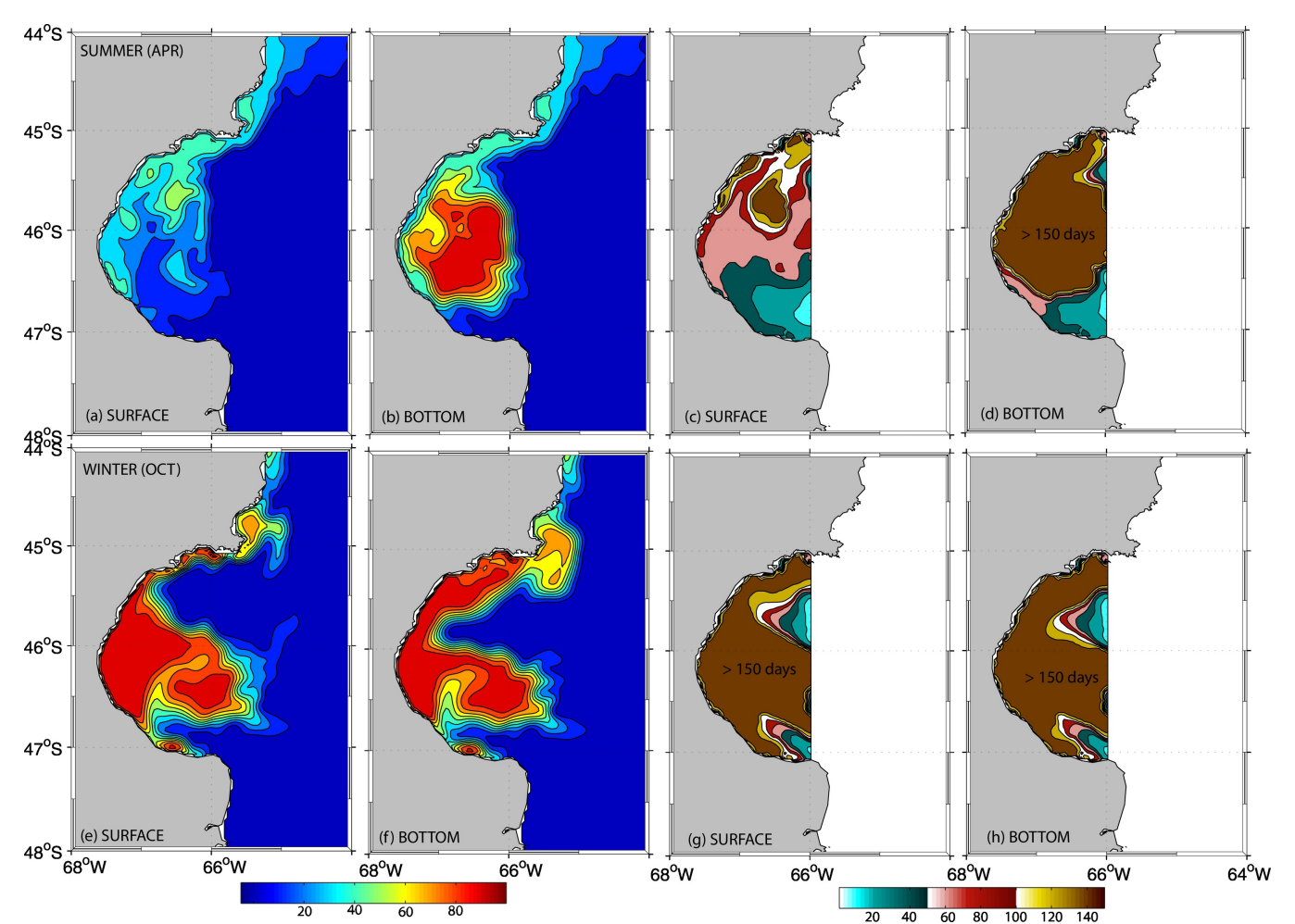
SUMMER (APR)
(a) SURFACE
(b) BOTTOM
(c) SURFACE
(d) BOTTOM
> 150 days
WINTER (OCT)
(e) SURFACE
(f) BOTTOM
(g) SURFACE
(h) BOTTOM
> 150 days
> 150 days
44°S
45°S
46°S
47°S
48°S
68°W
66°W
64°W
20
40
60
80
100
120
140

Figure 4

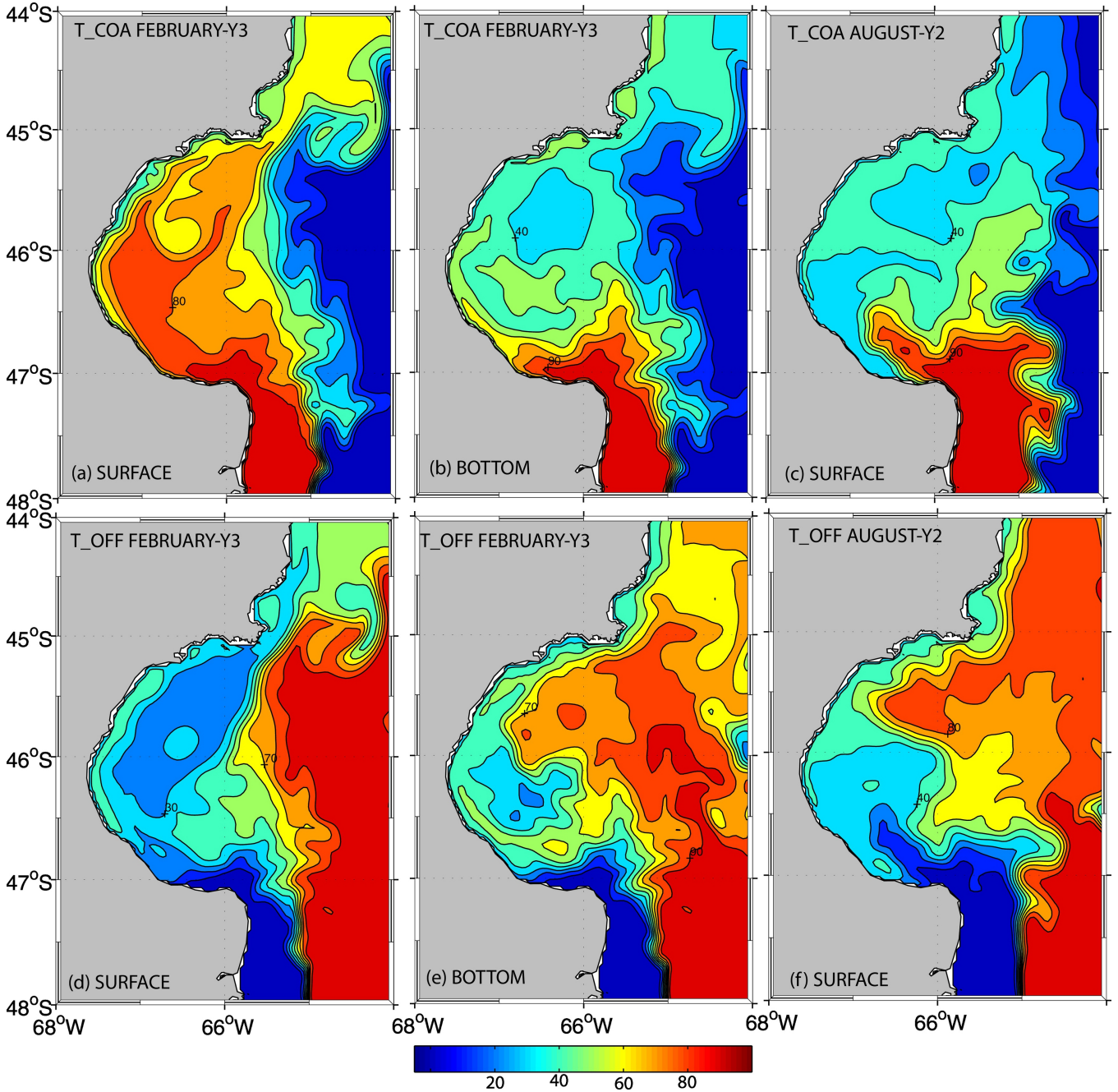
T_COA FEBRUARY-Y3
T_COA FEBRUARY-Y3
T_COA AUGUST-Y2
(a) SURFACE
(b) BOTTOM
(c) SURFACE
T_OFF FEBRUARY-Y3
T_OFF FEBRUARY-Y3
T_OFF AUGUST-Y2
(d) SURFACE
(e) BOTTOM
(f) SURFACE
44°S
45°S
46°S
47°S
48°S
68°W
66°W
20
40
60
80

Figure 5

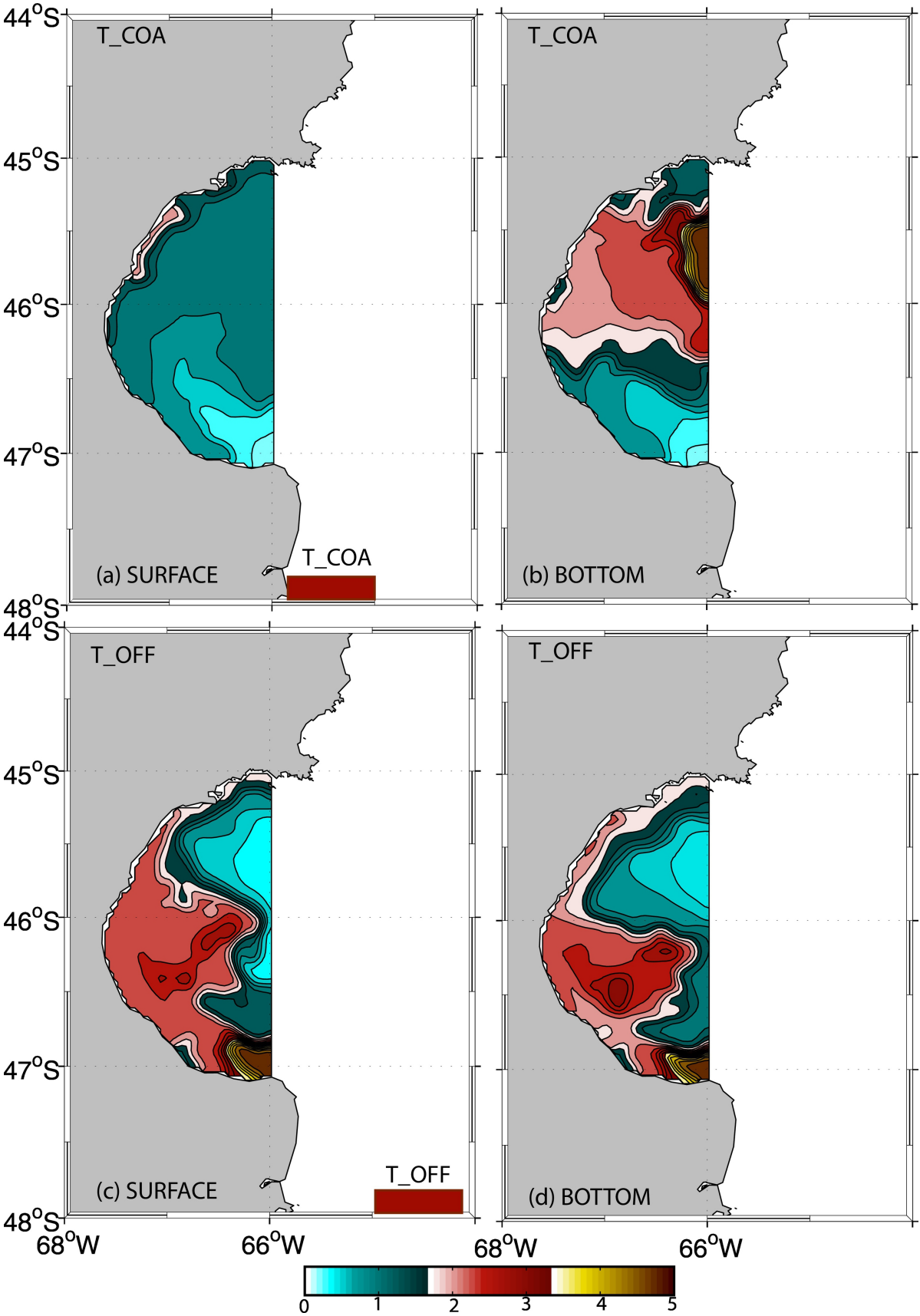
T_COA
T_COA
(a) SURFACE
T_COA
(b) BOTTOM
T_OFF
T_OFF
(c) SURFACE
T_OFF
(d) BOTTOM
44°S
45°S
46°S
47°S
48°S
68°W
66°W
0
1
2
3
4
5

Figure 6

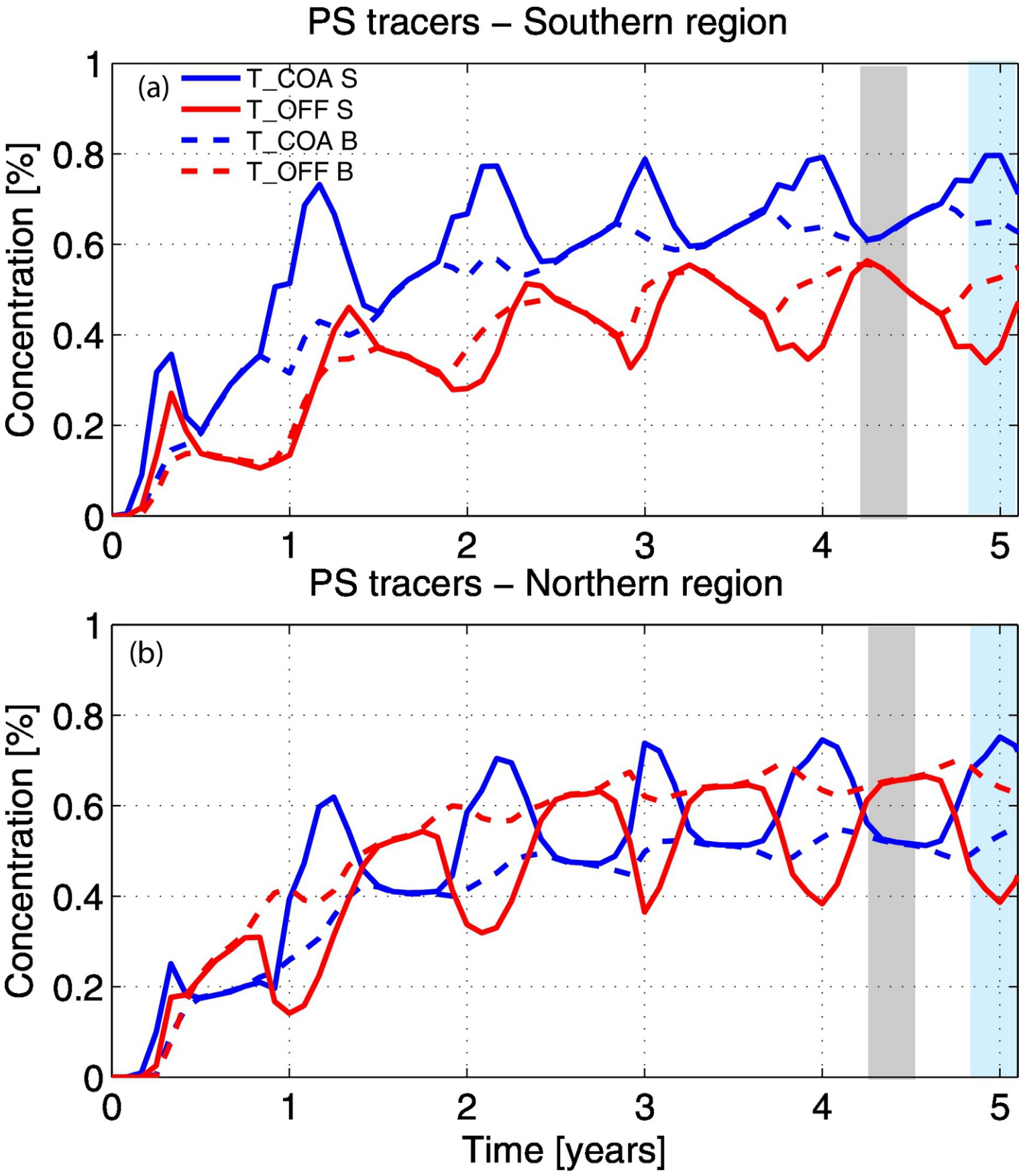
PS tracers – Southern region
(a)
T_COA S
T_OFF S
T_COA B
T_OFF B
Concentration [%]
0
0.2
0.4
0.6
0.8
1
0
1
2
3
4
5
PS tracers – Northern region
(b)
Concentration [%]
Time [years]

Figure 7

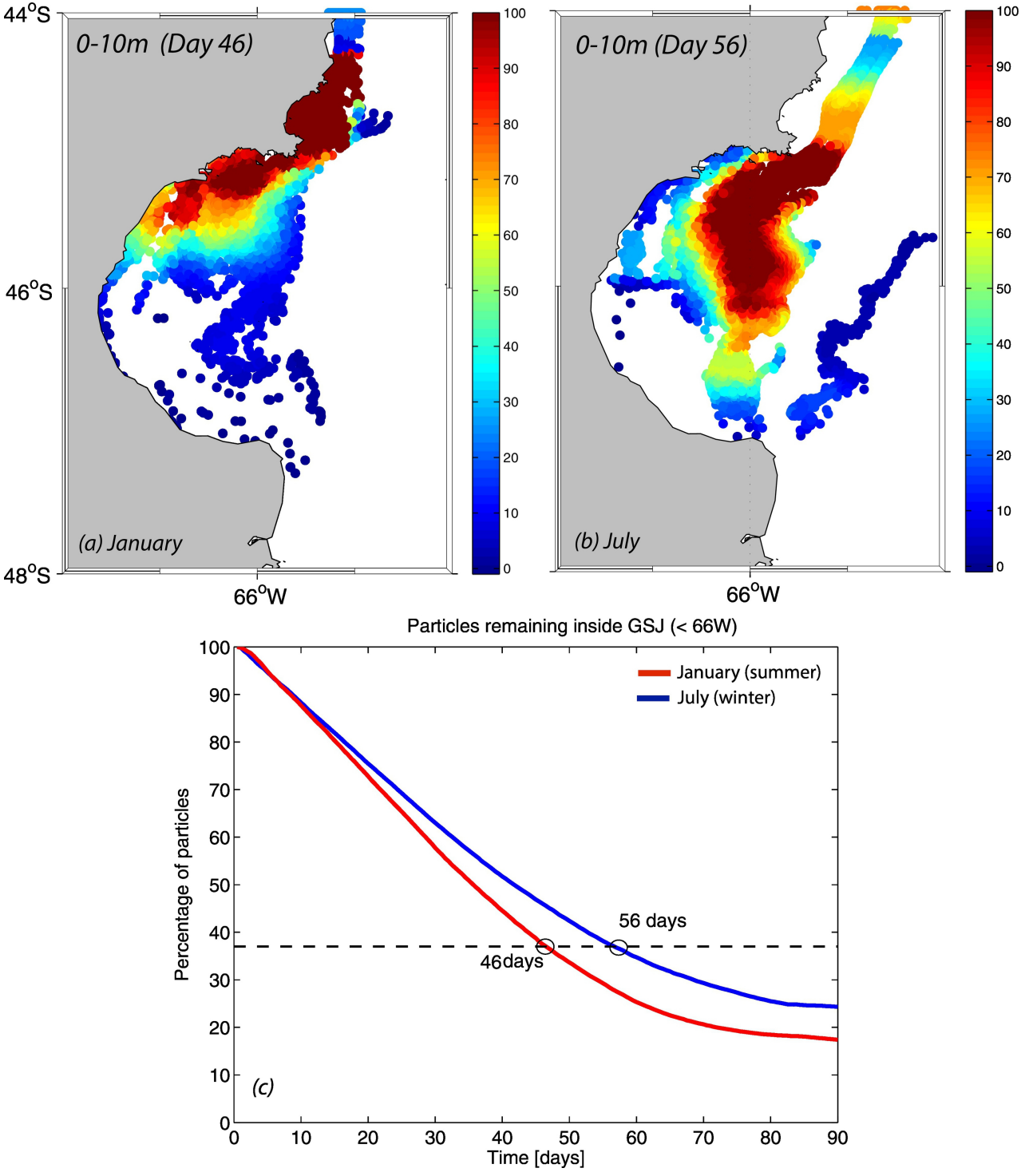
0-10m (Day 46)
(a) January
0-10m (Day 56)
(b) July
44°S
46°S
48°S
66°W
66°W
100
90
80
70
60
50
40
30
20
10
0
Particles remaining inside GSJ (< 66W)
January (summer)
July (winter)
Percentage of particles
56 days
46days
(c)
Time [days]

Figure 8

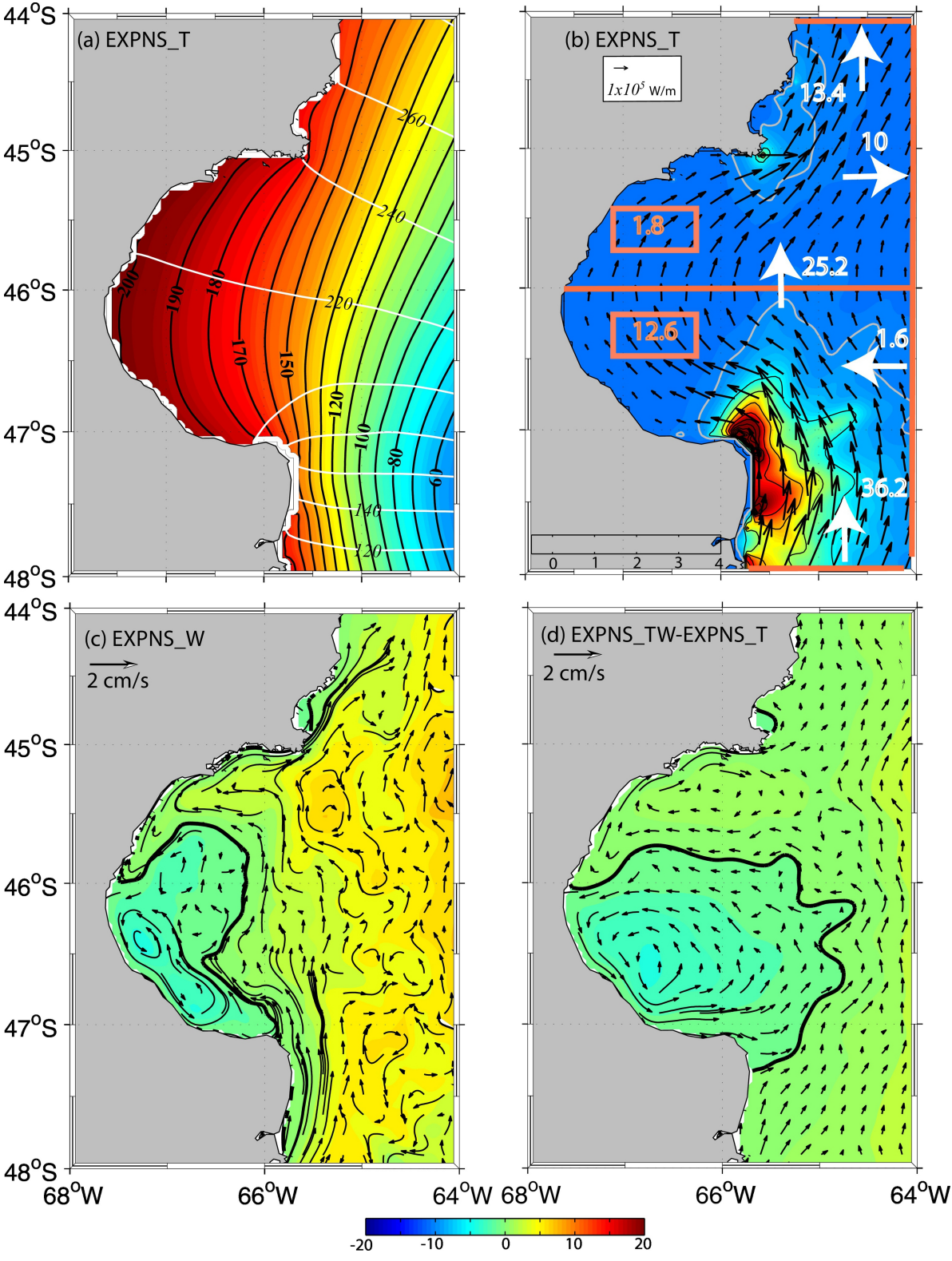
(a) EXPNS_T
(b) EXPNS_T
1x10^5 W/m
13.4
10
1.8
25.2
12.6
1.6
36.2
(c) EXPNS_W
2 cm/s
(d) EXPNS_TW-EXPNS_T
2 cm/s
44°S
45°S
46°S
47°S
48°S
68°W
66°W
64°W
-20
-10
0
10
20

Figure 9

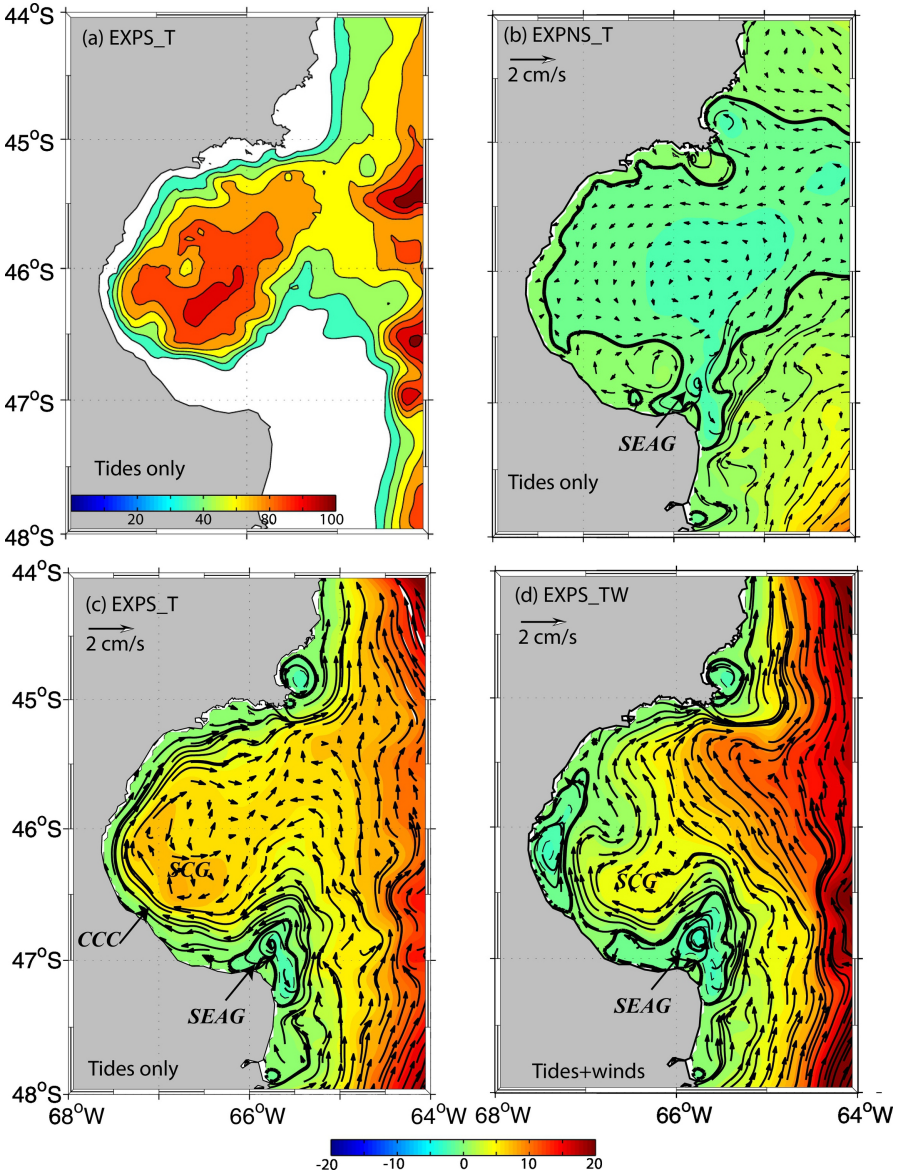
(a) EXPS_T
Tides only
20
40
80
100
(b) EXPNS_T
2 cm/s
SEAG
Tides only
(c) EXPS_T
2 cm/s
SCG
CCC
SEAG
Tides only
(d) EXPS_TW
2 cm/s
SCG
SEAG
Tides+winds
44°S
45°S
46°S
47°S
48°S
68°W
66°W
64°W
-20
-10
0
10
20

Figure 10

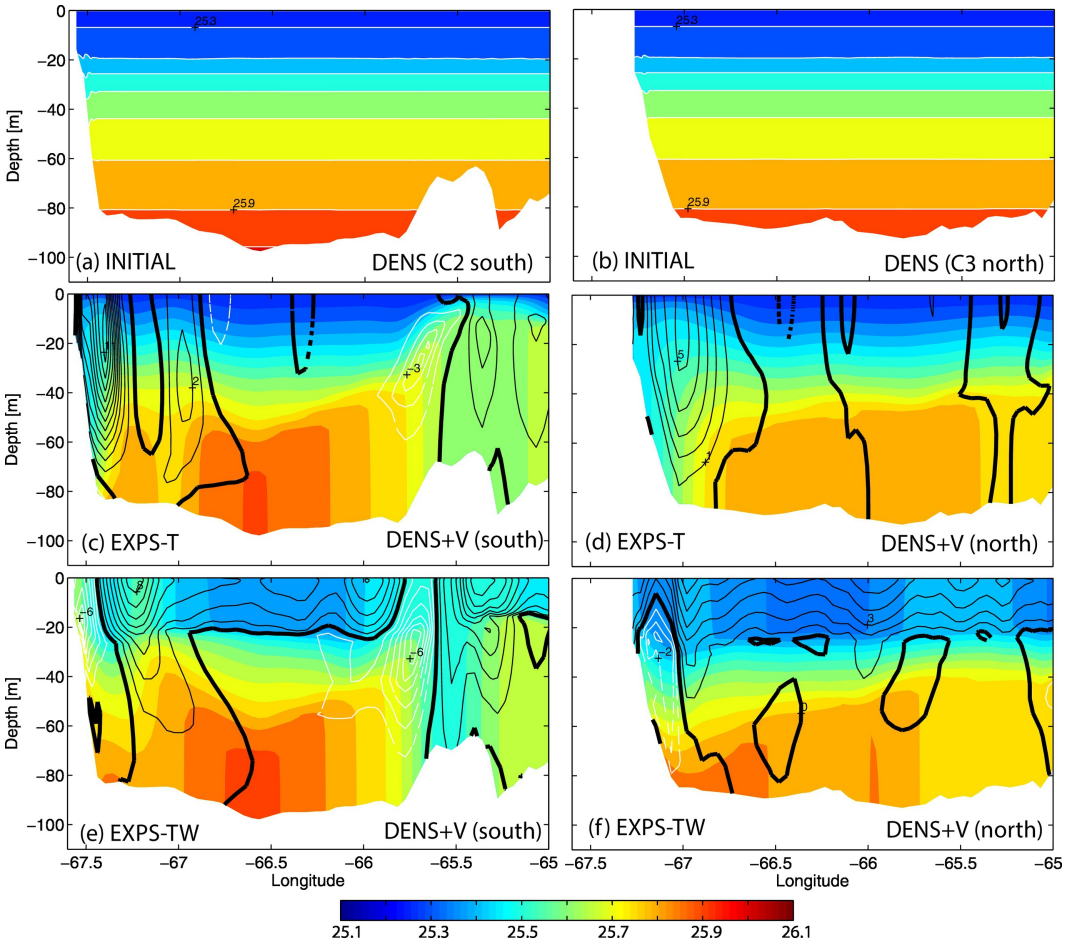
Depth [m]
0
−20
−40
−60
−80
−100
25.3
25.9
(a) INITIAL
DENS (C2 south)
(b) INITIAL
DENS (C3 north)
(c) EXPS-T
DENS+V (south)
(d) EXPS-T
DENS+V (north)
(e) EXPS-TW
DENS+V (south)
(f) EXPS-TW
DENS+V (north)
−67.5
−67
−66.5
−66
−65.5
−65
Longitude
25.1
25.3
25.5
25.7
25.9
26.1

Figure 11

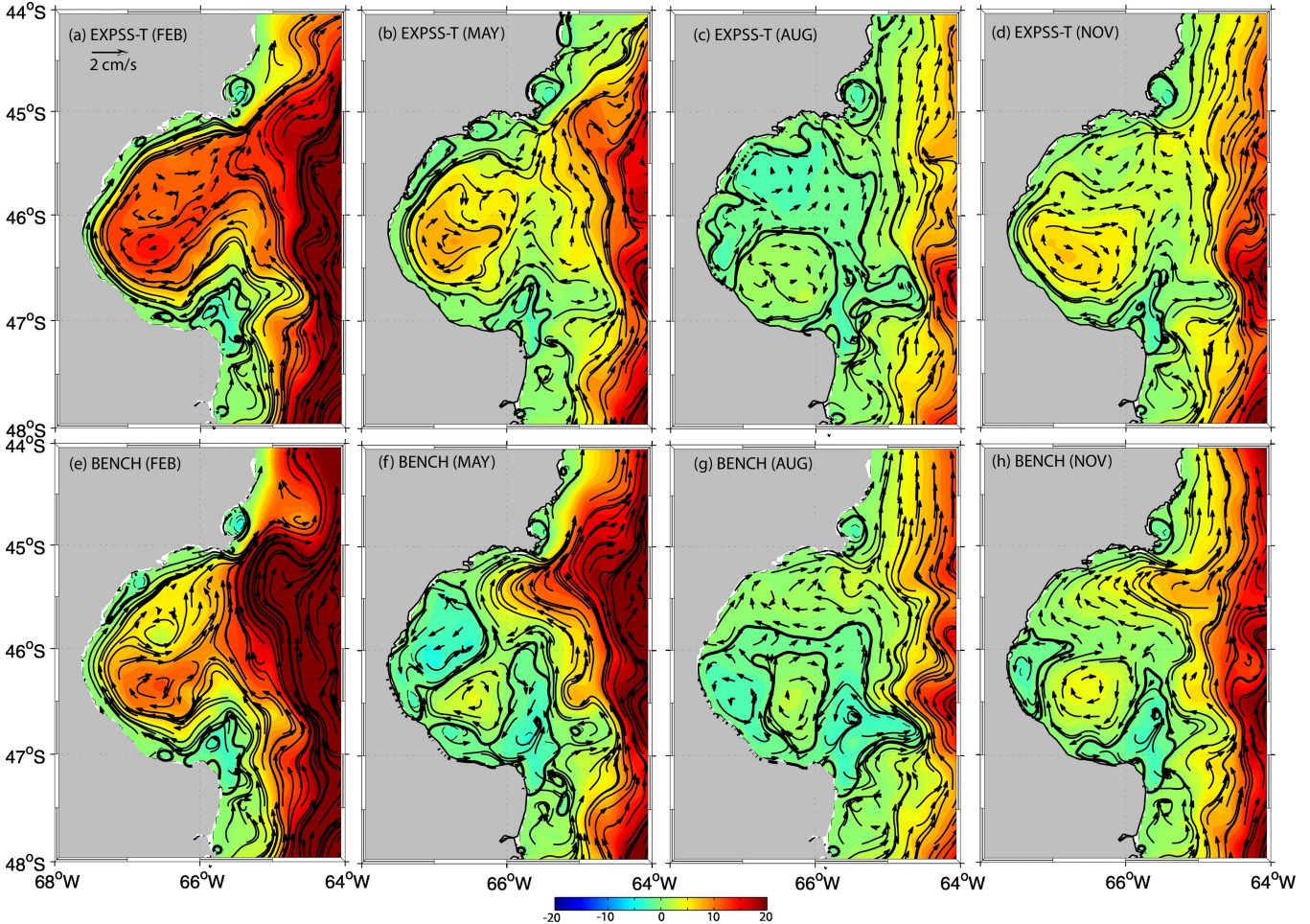
(a) EXPSS-T (FEB)
2 cm/s
(b) EXPSS-T (MAY)
(c) EXPSS-T (AUG)
(d) EXPSS-T (NOV)
(e) BENCH (FEB)
(f) BENCH (MAY)
(g) BENCH (AUG)
(h) BENCH (NOV)
44°S
45°S
46°S
47°S
48°S
68°W
66°W
64°W
-20
-10
0
10
20

Figure 12

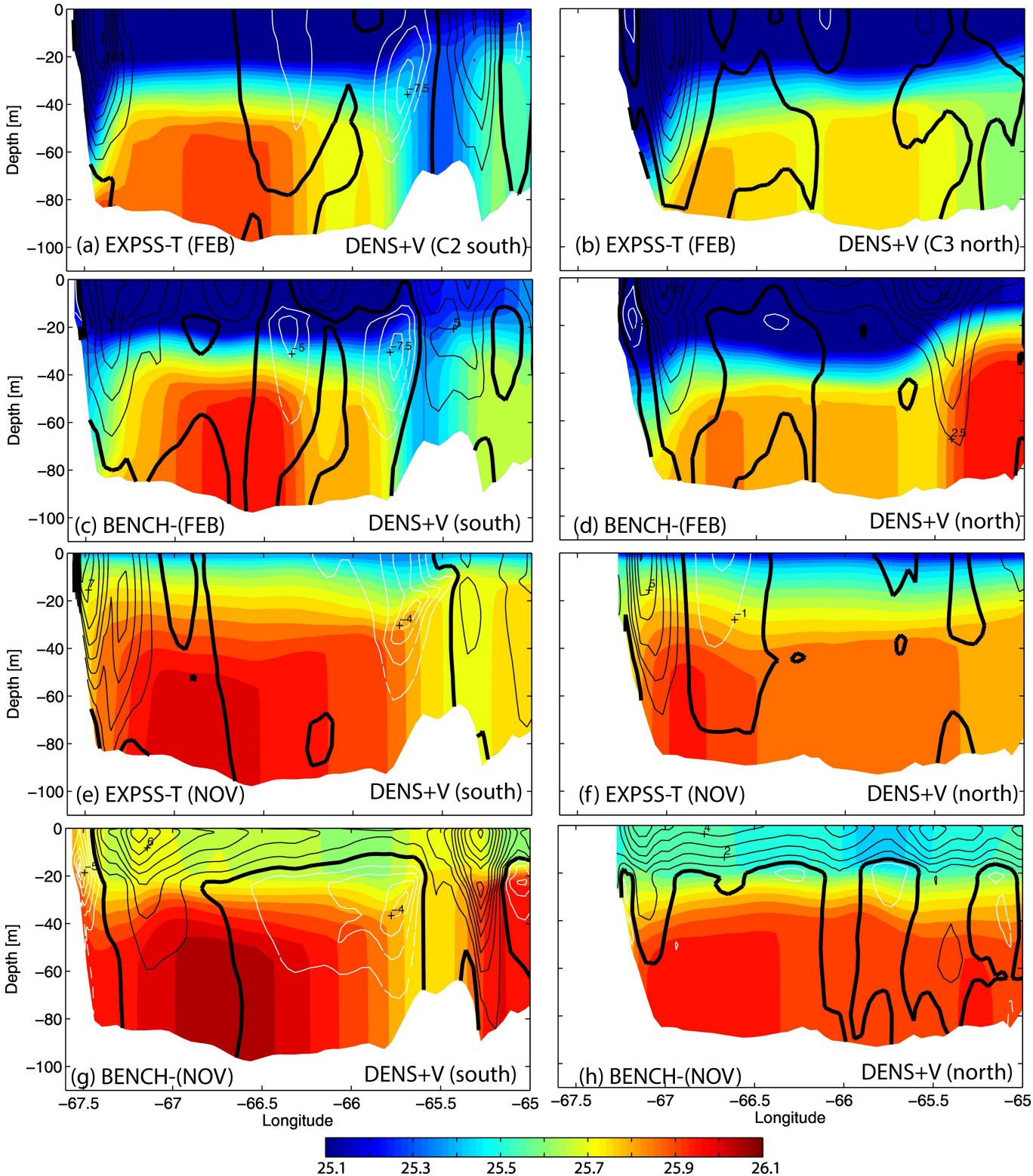
Depth [m]
0
−20
−40
−60
−80
−100
(a) EXPSS-T (FEB)
DENS+V (C2 south)
(b) EXPSS-T (FEB)
DENS+V (C3 north)
(c) BENCH-(FEB)
DENS+V (south)
(d) BENCH-(FEB)
DENS+V (north)
(e) EXPSS-T (NOV)
DENS+V (south)
(f) EXPSS-T (NOV)
DENS+V (north)
(g) BENCH-(NOV)
DENS+V (south)
(h) BENCH-(NOV)
DENS+V (north)
−67.5
−67
−66.5
−66
−65.5
−65
Longitude
25.1
25.3
25.5
25.7
25.9
26.1

Figure 13

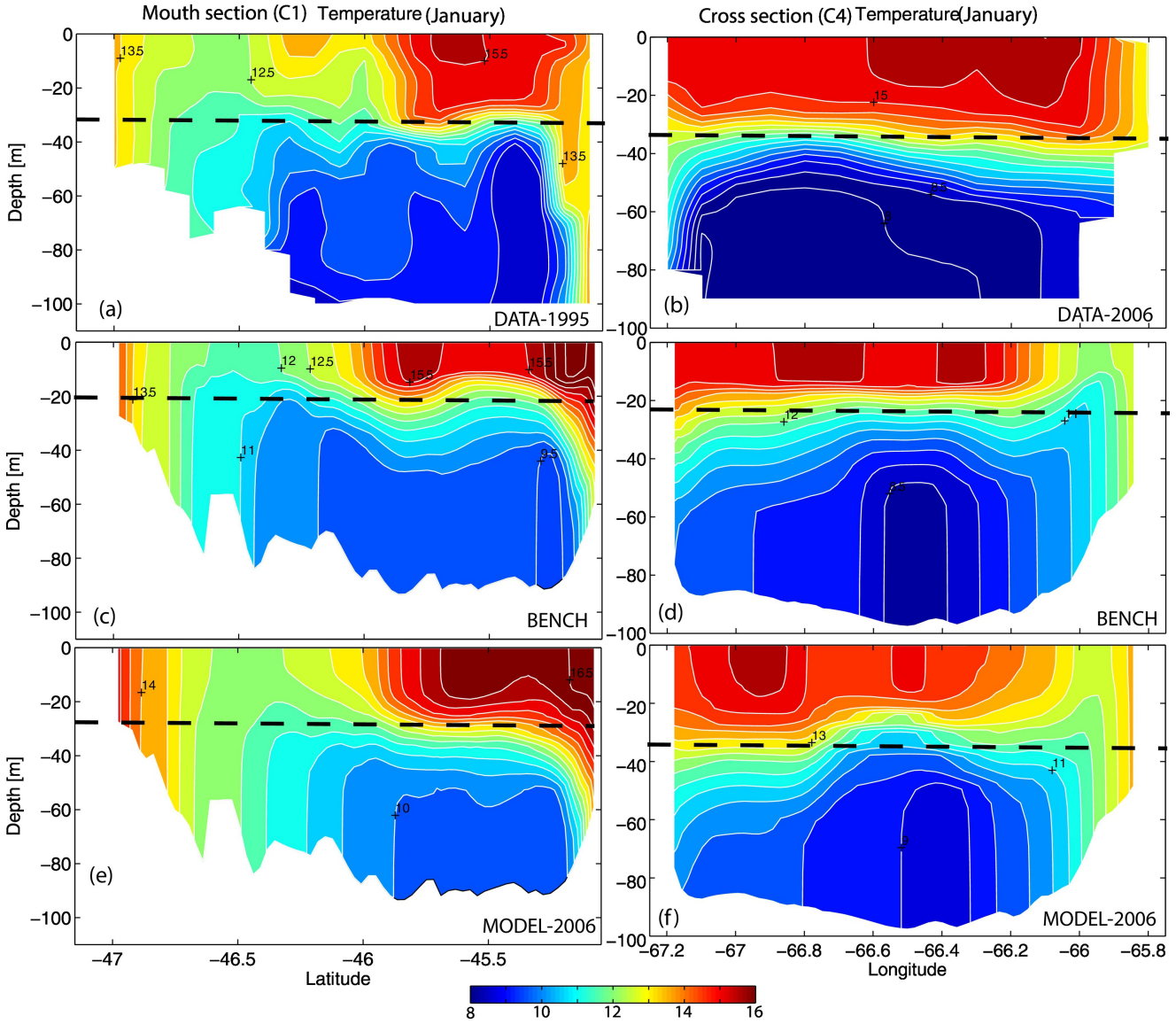
Mouth section (C1) Temperature (January)
Cross section (C4) Temperature (January)
Depth [m]
Latitude
Longitude
(a)
DATA-1995
(b)
DATA-2006
(c)
BENCH
(d)
BENCH
(e)
MODEL-2006
(f)
MODEL-2006
8
10
12
14
16

Figure 14